SUPPORTING INFORMATION

Sustainable NO_x production from air in pulsed plasma: Elucidating the chemistry behind the low energy consumption

Elise Vervloessem,*[a,b] Yury Gorbanev [a], Anton Nikiforov[b],

Nathalie De Geyter[b] and Annemie Bogaerts[a]

[a] University of Antwerp, Universiteitsplein 1, 2610 Antwerp, Belgium

[b] Ghent University, Sint-Pietersnieuwstraat 25, 9000 Ghent, Belgium

Table of Contents

S.1 Details on the experimental setup

S.1.1 Voltage and Current Waveforms – Pulsing Behaviour in the Soft Jet

Fig. S.1 shows the V-I characteristics of the Soft Jet at three relevant time scales: (a) long, (b) for a typical gas residence time at 1 L/min, (c) short. The power deposited in the plasma (estimated from **Fig. S.1c**) was calculated as described previously.[1] Because of the spark type nature of the plasma, the plasma is formed only during the peak of the voltage and current waveform (**Fig. S.1c**), as explained in **section 2.1** of the main text. Hence, this corresponds to the discharge power, which is deposited into the plasma, whereas the sinusoidal shape of the current and voltage waveforms correspond to a displacement current (not going into the plasma)**.**[2,3] It has to be emphasized here that this plasma power is used for the calculation of the energy consumption of NO_x production.[4]

The multiplication of the current and voltage waveforms (**Fig. S.1c**) gives a power profile as a function of time, shown in **Fig. S.1d**. The integration of the peak in this power profile, corresponding to the voltage and current peaks (i.e. the sharp peak above the sinusoidal-like shape in **Fig. S.1d**) gives an energy of ca. $4 \cdot 10^{-6}$ J, which, when divided by the duration of the peak (0.74 μs), yields a power value (in W) corresponding to the time-averaged power within the peak. This way, the average power of two peaks within the same period was found to be 5.11 ± 0.35 W. For a volume of 0.39 mm^3, this results in a peak power density of 13 $kW.cm^{-3}$ (i.e. the power density for the 0.74 μs duration of the pulse).

The asymmetry of the power profile shown in **Fig. S.1d** is explained by a higher power deposition in the positive half-period of the applied voltage. Such effect of the voltage polarity on the discharge behaviour is often observed in plasmas[5] and can be explained by an effect of charge accumulation in the discharge gap leading to asymmetry of the V-I waveforms.

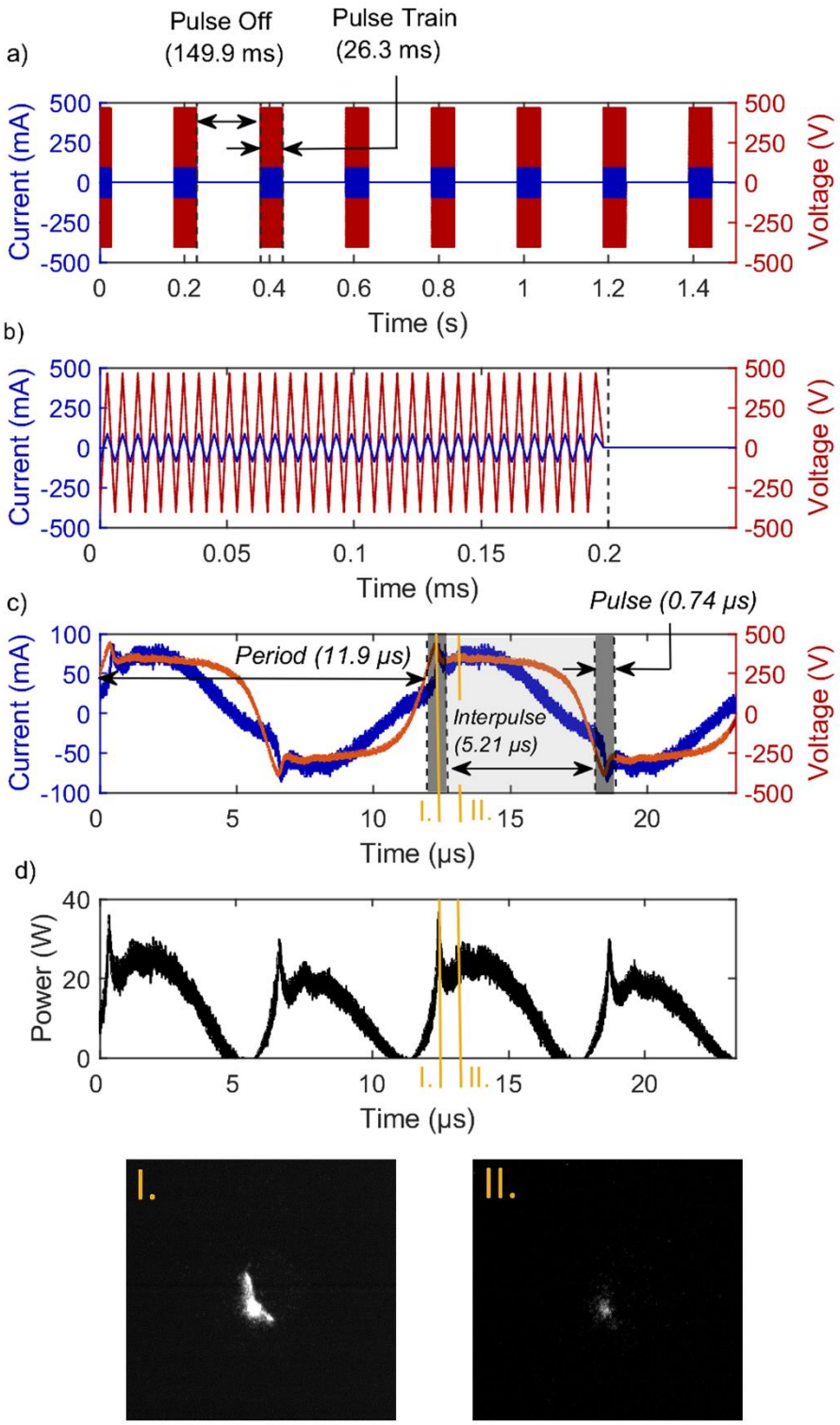
a)
Pulse Off
(149.9 ms)
Pulse Train
(26.3 ms)
Current (mA)
Voltage (V)
Time (s)
b)
Current (mA)
Voltage (V)
Time (ms)
c)
Pulse (0.74 μs)
Period (11.9 μs)
Interpulse
(5.21 μs)
Current (mA)
Voltage (V)
Time (μs)
d)
Power (W)
Time (μs)
I.
II.

Fig. S.1 Measured current and voltage characteristics of the Soft Jet in dry air, in the relevant time scales. (a) Long time scale, showing the pulse trains with pulse-off times. (b) Representation of a typical residence time of gas molecules in the plasma (here for 1 L/min). During this residence time (0.2 ms), the molecules experience ca. 30 pulses (at 1 L/min) within one pulse train. (c) Applied voltage and current, and (d) resulting power, for a few pulses, showing in (c) the pulse (dark grey) – interpulse (light grey) characteristics within a pulse train. There are 4420 pulses within one pulse train. The power profile is obtained by multiplying the voltage and current. Within the sharp peaks, the actual low current plasma spark is formed. I. and II. are two time-resolved images of the plasma discharge obtained using a Hamamatsu C8484 ICCD camera[6] with a 100 ns exposure time and the camera lens surface perpendicular to the effluent. Plasma conditions: 1 L/min, N_2. In I., the intense arc shape corresponds to a plasma arc, II. shows a visible round shaped zone of low light intensity appearing in between plasma arc corresponding to the afterglow emission.

To calculate the power absorbed in the plasma, only the plasma pulse duration is considered, which is the general approach used in plasma research. To clarify this concept, **Figure S.2** shows an overview of the power deposition in the device. Panel (a) shows the energy consumed by the plasma source and consumed by the power supply. Maximising the amount of power consumed by plasma generation is a (power supply) engineering problem, which is out of the scope of our work. Panel (b) shows the power consumed by the plasma generation, which can be split up into two ways of power deposition:

(1) Power lost during the interpulse duration. This so-called *dark discharge* power can be reduced by V/I waveform optimisation, which is a physical/electrical engineering question.[7]

(2) Power going into the pulse. This is the power determining the chemical efficiency of the device and the focus of our work. It can be influenced by, for example, the pulse frequency and duration, which in turn will influence the chemical processes taking place within the plasma.”.

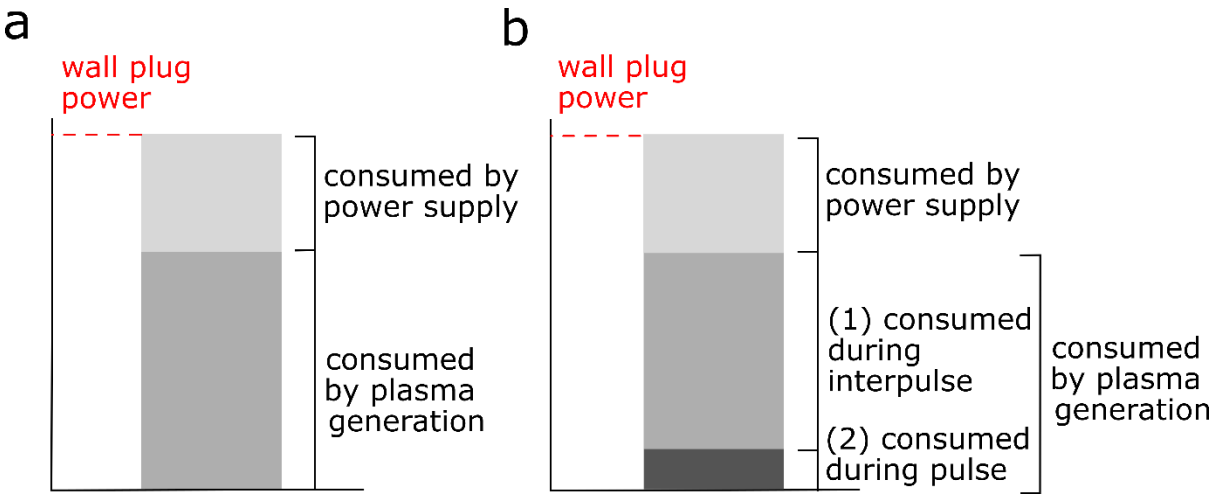

Fig. S.2 Division of the wall plug power put into the device: (a) engineering point of view, (b) plasma physics and plasma chemistry point of view. The red dashed line indicates the (total) wall plug power.

S.1.2 Temperature Measurements of the Plasma Arc and the Afterglow

Two types of temperature measurements were performed (both methods are explained in full in Ref 17):

(1) The plasma temperature through OES[8], a spatially- and time-averaged measurement which allowed us to measure the plasma core temperature (gas temperature in the arc) by a line of sight looking straight into the Soft Jet. It has to be indicated that the arc emission is much higher compared with the afterglow emission so the contribution of the emission from the afterglow in the gas temperature estimations was very low or even negligible.

(2) The gas temperature outside of the jet (the afterglow) through Rayleigh-scattering. This part of the work only deals with an estimation of the gas temperature in the afterglow with no contribution of the arc emission.

These two methods are complementary; one is used to study the gas heating in the arc and the other in the afterglow. Method (1) cannot be used to determine the gas temperature in the afterglow due to the low emission, and method (2) cannot be used to measure the arc temperature due to geometric constraints.

Fig. S.3 shows the normal plasma effluent, in the absence of a thermocouple (a), as well as the broadening of the plasma effluent (b) and the arcing (c) onto the thermocouple, rendering the measurements invalid.

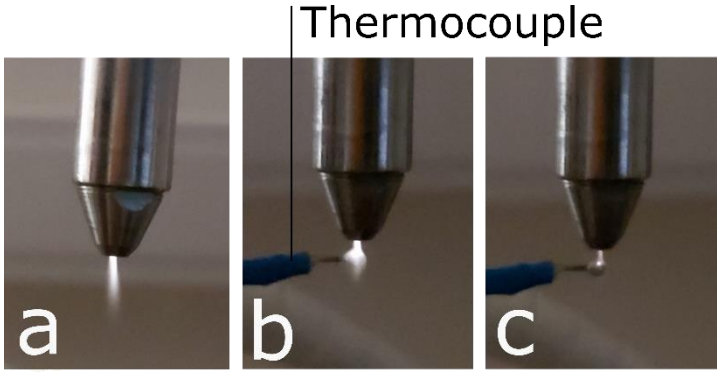

Figure S.3 (a) The Soft Jet in operation, (b) with a thermocouple placed in the afterglow to measure the temperature, the gas dynamics are changed significantly, resulting in widening of the afterglow shape and (c) with a thermocouple placed closer to the nozzle tip, arc formation is visible onto the thermocouple.

S.2 The quasi-1D model

The quasi-1D model of the Soft Jet was developed based on a 0D model (section **S.2.1** and **S.2.2**) coupled with a computational fluid dynamics (CFD) model (section **S.2.3**). This allows the proper translation of a time-dependent 0D model to a position-dependent quasi-1D model, as described in detail in sections **S.2.2.1** and **S.2.2.2**.

S.2.1 0D model – The base for the quasi-1D model

To gain insight into the plasma chemistry, we developed a zero-dimensional (0D) chemical kinetics model within the code ZDPlasKin. Herein, the species densities are obtained as a function of time by numerically solving the continuity equation (**equation 1)** for the individual species included in the model (see **Table 1** in the main paper):

$$\frac{\mathrm{dn_i}}{\mathrm{dt}} = \sum_{\mathrm{j}} \left[\left(\mathrm{a_{ij}^R} - \mathrm{a_{ij}^L} \right) \mathrm{k_j} \prod_{\mathrm{l}} \mathrm{n_l^L} \right] \tag{1}$$

n_i is the density of species i, a_{ij}^R and a_{ij}^L are the right and left stoichiometric coefficients species i in reaction j, for the following general reaction:

$$\mathrm{aA} + \mathrm{bB}\ (+\Delta\mathrm{H}) \overset{\mathrm{k_j}}{\rightarrow} \mathrm{cC} + \mathrm{dD}\ (+\Delta\mathrm{H}) \tag{2}$$

Here, A, B, C and D are the different species and a, b, c and d are their respective stoichiometric coefficients. ΔH represents the enthalpy of reaction j. The reaction rate coefficients, k_j, of the heavy particle reactions are expressed in $\mathrm{cm^3\ s^{-1}}$ or $\mathrm{cm^6\ s^{-1}}$ for two-body or three-body reactions, respectively. k_j is either constant or dependent on the gas temperature. The rate coefficients of the electron impact reactions are calculated according to the following equation:

$$\mathrm{k_i} = \int_{\varepsilon_{\mathrm{th}}}^{\infty} \sigma_\mathrm{i}(\varepsilon)\mathrm{v}(\varepsilon)\mathrm{f}(\varepsilon)\mathrm{d}\varepsilon \tag{3}$$

ε is the electron energy (usually in eV), $\varepsilon_{\mathrm{th}}$ is the minimum threshold energy needed to induce the reaction, $\mathrm{v}(\varepsilon)$ the velocity of the electrons, $\sigma_\mathrm{i}(\varepsilon)$ is the cross section of collision i, and $\mathrm{f}(\varepsilon)$ is the electron energy distribution function (EEDF) (Elastic collisions are also included in the model: in this case, the lower limit of the integration equals 0.). To calculate the EEDF and the rate coefficients of the electron impact reactions, the code has a built-in Boltzmann solver, BOLSIG+.[9] The electric field (E)

is calculated from a given power density, using the so-called local field approximation[10]:

$$E = \sqrt{\frac{P}{\sigma}} \quad (4)$$

P is the input power density (W m^{-3}) and σ is the plasma conductivity (A V^{-1} m^{-1}), expressed as[10]:

$$\sigma = e\, n_e\, \mu_e \quad (5)$$

where n_e is the electron number density and μ_e the electron mobility.

Every time progression in the 0D model can be translated into position progression by means of the gas flow velocity. The gas flow velocity profile in the Soft Jet is determined by CFD calculations, as explained in **S.2.3**. This transforms a time-dependent 0D model into a quasi-1D model, where the plasma characteristics vary as a function of the distance travelled by the gas through the Soft Jet. A more detailed explanation of this transformation and the specific Soft Jet quasi-1D model is given in the next section.

S.2.2 The quasi-1D model applied to the Soft Jet

A molecule moving through the Soft Jet has a residence time ranging from 2 ms to 94 µs, for inlet flow rates ranging from 0.1 to 2.0 L/min, respectively. This means the molecule either experiences a part of a pulse train or moves through the jet during the plasma-off time (**Fig. S.1a**). The former results into plasma-induced reactions, the latter leaves the gas unchanged. The model only calculates the behaviour of molecules moving through the pulse train, the remaining fraction is taken into account by means of the treatment fraction, calculated in the next section.

S.2.2.1 Treatment Fraction

There are three options for the gas molecules moving through the Soft Jet. These options determine whether a gas molecule is plasma-treated or not, i.e. what is the effective treatment fraction:

(1) The gas molecule moves through the plasma zone when plasma is on i.e. it is plasma-treated during the pulse train. This case applies to approximately 14.9% of the molecules, based on the duty cycle of the pulse train (i.e., 26.3/(149.9 + 26.3)), see

Fig. S.2a. Note, this duty cycle should not be mistaken with the duty cycle of the entire system (1.9%), as explained in the main paper.

(2) The remainder of the gas molecules move through the plasma zone untreated (pulse-off time; ca. 85.1% calculated from 149.9/(149.9 + 26.3)).

(3) Besides the duty cycle of the pulse train, also the physical dimensions and shape of the ignited plasma play a role in determining the effective treatment fraction. If the gas molecule moves alongside the plasma, it cannot be plasma-treated, regardless of the plasma ignition state. ICCD (Intensified Charged Coupled Device) camera images of the plasma recorded in our previous work[1] show what fraction of the cavity is taken up by the plasma. Based on this, we estimated that ca. 20% of the gas moving through the cavity during plasma-on time (case 1) is actually plasma-treated. From these 2D images of a 3D arc, it is only possible to estimate the fraction. However, this estimation does not influence the underlying mechanisms or other insights gained from the model, as it only decreases the plasma-treated fraction, not the way in which the gas is treated.

The effective treatment fraction is calculated by multiplying the duty cycle of the pulse train (case 1) with the fraction of the cavity that is taken up by plasma (case 3) and amounts to 3.0% (20% x 14.9%).
In practice, only case (1) is modelled, i.e. molecules moving through the Soft Jet when the plasma is on. Afterwards, the calculated densities of the various reactive plasma species (i.e., electrons, various ions, radicals, excited molecules) are multiplied by the effective treatment fraction (3.0%) to obtain the effective calculated species densities. Indeed, the remainder of the molecules move through untreated by the plasma, hence they are not converted into reactive plasma species.

S.2.2.2 Quasi-1D model of the species moving through the plasma

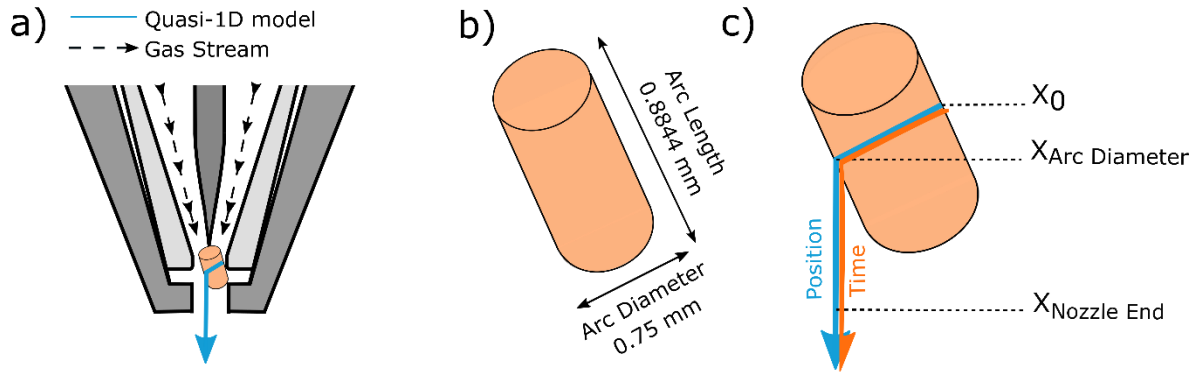

Fig. S.4 Schematic description of the geometry considered in the quasi-1D model. The dashed lines in (a) indicate the gas flow, the blue lines in (a, c) indicate the region of the simulation. (a) Soft Jet, with the plasma arc represented as a cylinder. (b) Dimensions of this plasma arc cylinder. (c) Schematic explanation of the quasi-1D model: the gas enters the plasma arc region at X_0 and leaves the arc at $X_{Arc\ Diameter}$, after which it continues its way through the nozzle and in the afterglow. Hence, the model follows a volume element, moving through the plasma and the afterglow.

The molecules in the quasi-1D model follow the blue line (**Fig. S.4**), through the plasma where the molecules experience a pulse train, into the afterglow and outside of the jet until a steady state is reached. Two measured plasma parameters were used as input in the model: *a power profile and a gas temperature profile*. Together they define the pulsed behaviour of the jet and the conditions inside and outside of the jet (see **Fig. 4a** of the main paper).

(a) Power profile – In plasma

The power profile was constructed based on the V-I measurements of the Soft Jet during a pulse train (**Fig. S.1c,d**). The plasma pulse duration of 0.74 µs followed by an interpulse of 5.21 µs was considered in the model, resulting in a pulse period of 5.95 µs. The peak power dissipated in the discharge was calculated according to **Fig. S.1d**, taking into account the average area under the peaks (5.11 W). Although the interpulse power (density) profile is not known, we know that the power does not reach zero in the interpulse period (**Fig. S.1d**). Therefore, we assumed that the interpulse power is 10% of the peak power. This assumption also significantly improves the robustness of the calculations, as going to zero power, on the small timescale that is

necessary for the Soft Jet's calculations, makes the model crash, unless very small timesteps are used, resulting in much longer calculation times.

Note that making elaborate speculations about the exact shape of the interpulse power profile would not affect the calculation results, but would only impede the model operation and interpretation. Therefore, we decided upon a constant interpulse power, that includes the known characteristics of the power, preventing that the results interpretation would become ambiguous.

(b) Gas temperature profile – In plasma

The gas temperature profile in the plasma is based on optical emission spectroscopy (OES) measurements and is virtually independent of flow rate in the range used here, as reported in our recent work.[1] The temperature during the pulse, i.e. the temperature of the plasma arc, was measured to be 1750 $\pm$ 150 K and coincides with the power peak. During the interpulse, an exponential decay to 330 K is set in accordance with the average gas temperature measured by Rayleigh scattering in the afterglow (**Figure 4a**; main paper).[1] The shape of the temperature decay in between pulses was estimated based on a sensitivity study where we tested four different profiles, shown in **Fig. S.5**: a slow linear drop (profile 1), an exponential drop (profile 2), a fast linear drop (profile 3) and a straight vertical drop after the pulse ends (profile 4). Profiles 1 and 4 act as limiting cases to estimate the influence of the temperature drop on the modelling results. The modelling results do not differ significantly for the different interpulse temperature profiles. We therefore chose the more intuitive profile 2, which is exponential.

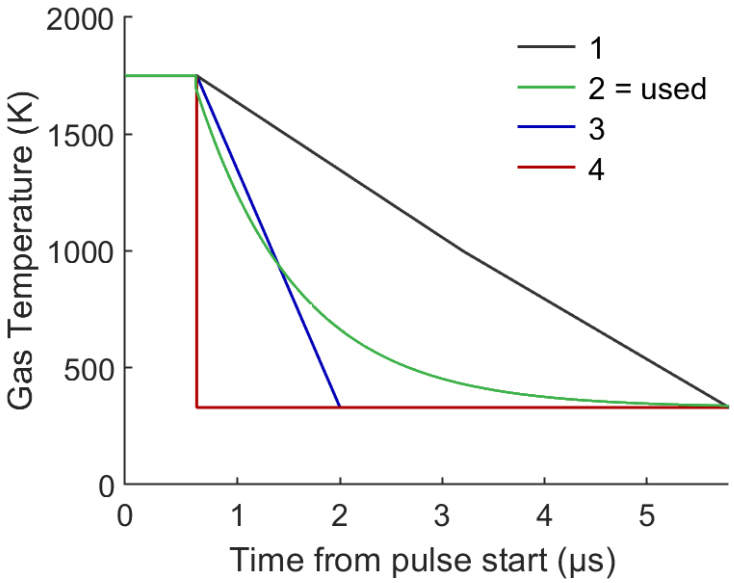

Fig. S.5 Four options of gas temperature as a function of time from the pulse start until the start of a new pulse, considered in the model: (1) slow linear drop, (2) exponential drop, (3) fast linear drop and (4) instantaneous drop.

(c) Power and gas temperature profile – Outside plasma

Finally, after the pulse train, the species move into the post-plasma zone, where the gas temperature (T_g) rapidly decreases to room temperature and the power was set to zero (no plasma). The gas temperature was calculated from Rayleigh scattering measurements at two distances from the nozzle tip (1.2 and 3.4 mm) and four different flow rates (0.2; 0.35; 0.7; and 1.4 L/min) as described in our previous work.[1] Next to these data points, the gas temperature in the plasma arc (1740 K; 0 mm, obtained from OES; see previous section) and the temperature of the room (308 K; position of 10 mm) are also known. We used these four experimental data points to fit an exponentially decreasing curve for the four different flow rates (0.2; 0.35; 0.7; and 1.4 L/min; see **Fig. S.6b**), based on four parameters: $T_g = a \cdot \exp(-b \cdot x) + c \cdot \exp(-d \cdot x)$, with x = the distance from the nozzle tip. Because of the strong difference in temperature between the plasma and the temperature at 10 mm from the nozzle (308 K) the temperature profiles in the afterglow are very alike for the four flow rates (0.2; 0.35; 0.7 and 1.4 L/min). For the other flow rates between 0.1 and 2.0 L/min an average fit (**Fig. S.6**; black dashed line) was used, based on the experimental data points. To validate this approximation to reality (i.e. a different temperature decay for each flow rate), we compared the calculated densities obtained when using the fitted

temperature profile based on the experimental data for that specific flow rate with the average fit. There was no significant difference between both approaches, so it is a valid assumption to use the average fit for all flow rates.

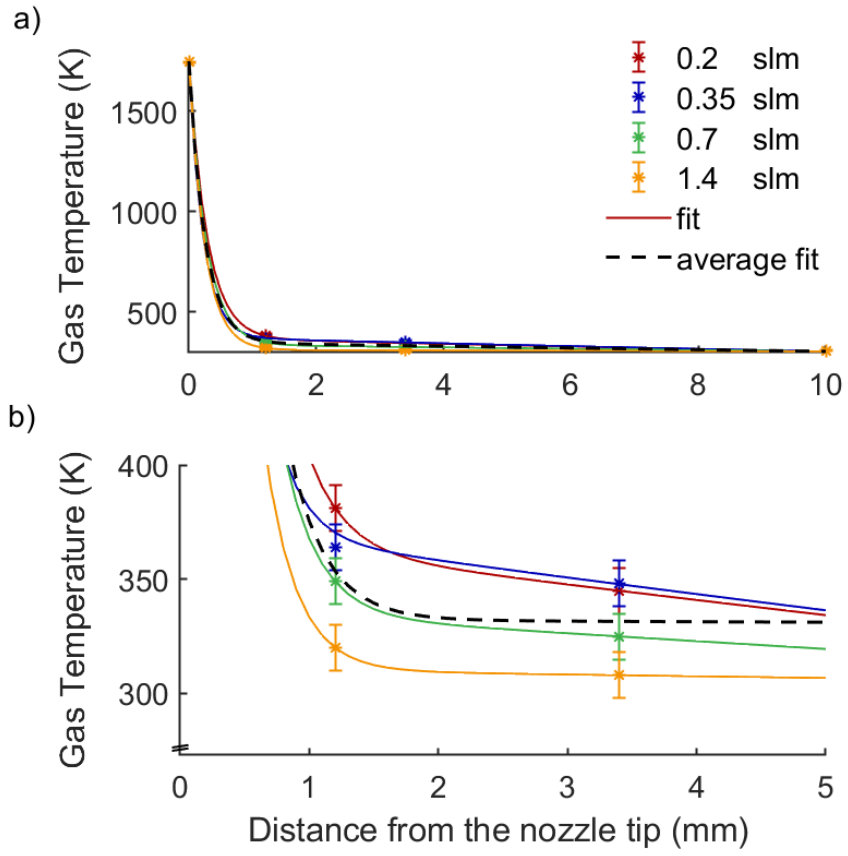

Fig. S.6 Gas temperature in the afterglow as measured by Rayleigh scattering experiments at 0.2, 0.35, 0.7 and 1.4 L.min^{-1} (stars), as a function of distance from the nozzle tip, as well as the temperature in the plasma (0 mm; 1750 K) and room temperature (10 mm; 308 K).[11] (a) Entire temperature profile from the plasma region until the simulation end (10 mm). (b) Zoomed into the points measured by Rayleigh scattering.

S.2.3 CFD simulations

The Soft Jet is cylindrically symmetrical, and its 2D geometry, considered in the CFD simulations, is shown in **Fig. S.7**. The 1D velocity profiles through the Soft Jet (**Fig. S.8**) are used to accurately transform the time-dependent simulation of the 0D model into a position-dependent one (quasi-1D model). The CFD calculations are performed until steady state is reached for each inlet flow rate, by means of a 2D axisymmetric turbulent gas $\kappa - \varepsilon$ model built in COMSOL Multiphysics.[12] The turbulent flow model results are used as input into the 0D model. It is independent of the plasma chemistry, i.e. we assume the flow is independent of the heat produced by the plasma or by

changes in the gas composition due to chemical reactions. This is a valid assumption, as the spatially averaged gas temperature does not exceed 350 K; hence, the influence of the gas heating on the flow behaviour is small compared with the background flow, and the conversion is too limited (<< 1 %) to cause any significant changes to the gas composition, and thus to the physico-chemical properties of the flow.

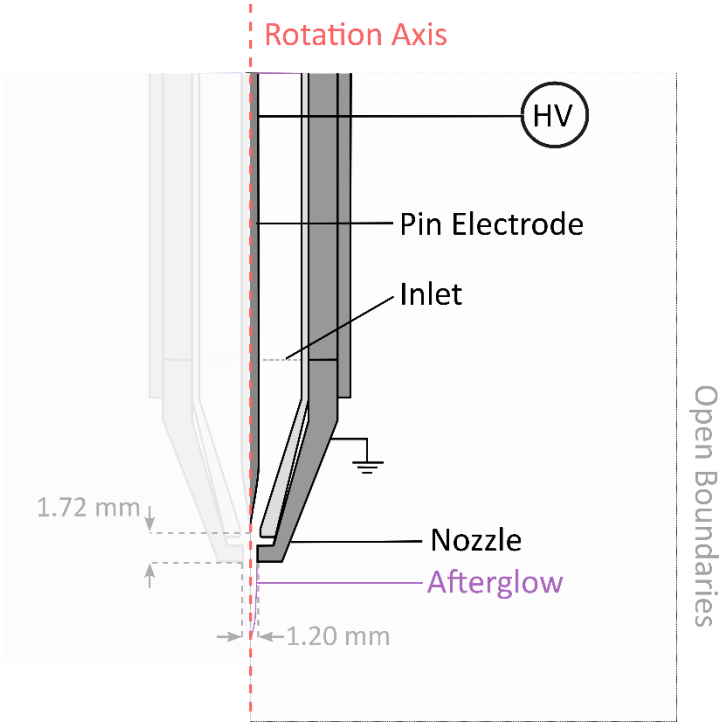

Fig. S.7 Geometry of the Soft Jet, used in COMSOL for the CFD calculations. The indication of the afterglow shape is used to ensure proper meshing around the outlet.

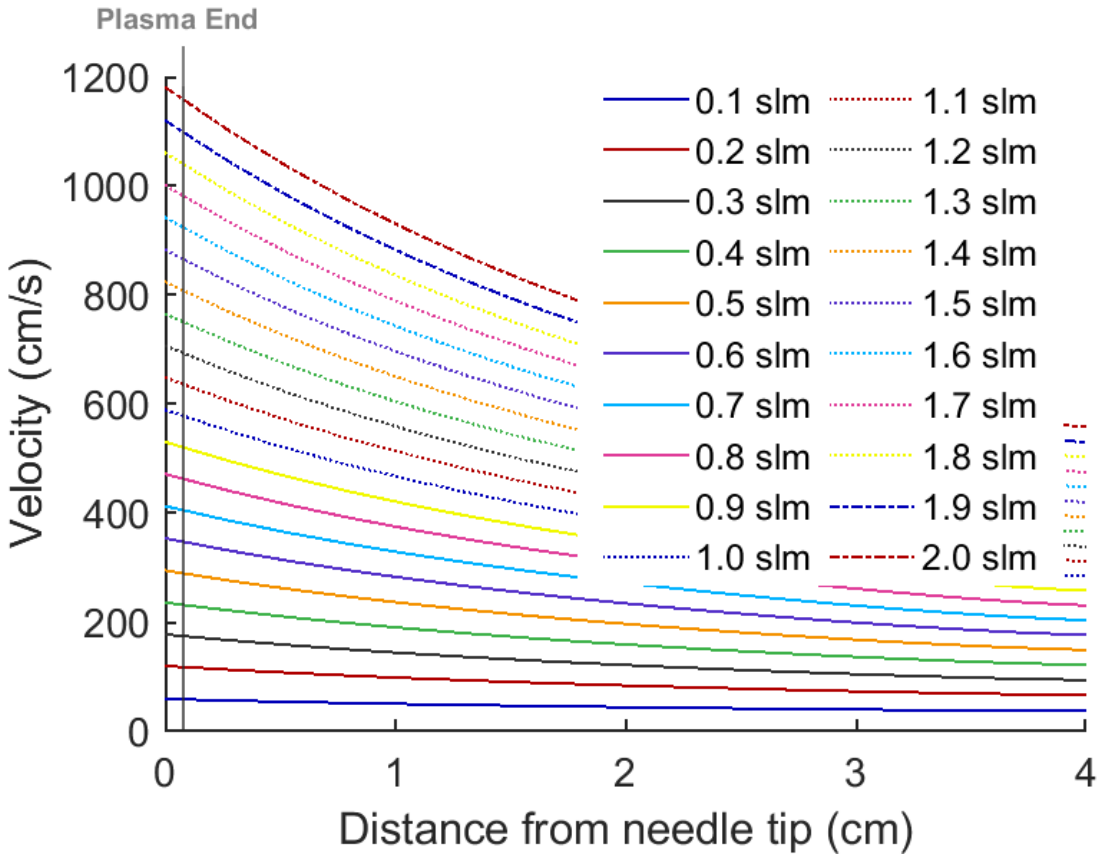

Fig. S.8 Axial gas velocity calculated via CFD simulations as a function of distance from the needle tip, for inlet flow rates of 2.0 – 0.1 L/min. The plasma end is indicated by the grey line (0.075 cm).

Based on these calculations, the residence time in the plasma ranges from 2 ms to 94 µs, for inlet flow rates ranging from 0.1 to 2.0 L/min, respectively.

The radial-component of the gas velocity at the nozzle edge is << 0.1 m/s for all flow rates. Hence, we can safely assume that short-lived reactive species do not come in contact with ambient air before they are destroyed, and thus mixing with ambient air at the nozzle does not have to be included in the quasi-1D model.

S.2.4 Chemistry set included in the quasi-1D model

The set of reactions is based on a (revised) compilation of reactions reported in our previous work.[13] The set contains an elaborate description of the vibrational kinetics of N_2 and O_2, i.e. N_2 and O_2 electron impact vibrational excitations (e-V), N_2-N_2, O_2-O_2 and N_2-O_2 vibrational-vibrational (V-V) exchanges and N_2-N_2, N_2-O_2, O_2-N_2, O_2-O_2, N_2-N, O_2-O and N_2-O vibrational-translational (V-T) relaxations. 24 vibrational levels for N_2 and 15 levels for O_2 are included. Next to vibrational exchanges, the set includes electron impact, neutral-neutral, neutral-ion and ion-ion reactions. The species taken into account in the model are listed in **Table 1** of the main paper. This includes neutral molecules in the ground state, vibrationally and electronically excited states, various radicals, positive and negative ions, and electrons. **Table S.1** lists all electron impact reactions. Most of these reactions are treated by energy-dependent cross sections. **Table S.2** lists the neutral-neutral reactions and the corresponding rate coefficient expressions. For certain reactions, the rate coefficients of the vibrationally excited species are determined according to the Fridman-Macheret model, in which the activation energy is reduced by $\alpha\, E_v$, where α is the vibrational efficiency to lower the activation barrier and E_v is the vibrational energy. For those reactions, the α parameter is given in the last column of **Table S.3**. **Tables S.4 to S.6** list the electron-ion recombination, ion-neutral and ion-ion reactions and the corresponding rate coefficients, respectively. **Table S.7** lists the optical transitions.

This chemistry set was extensively developed and validated in our previous work.[13] After critical review of the literature, one reaction rate constant (k) in **Table S.2** (annotated in bold) was updated to a more recent k value from a reliable source. The Tables can be found at the end of the Supporting Information, under **Appendix**.

S.3. Extended information: Results and Discussion

S.3.1 Production rate

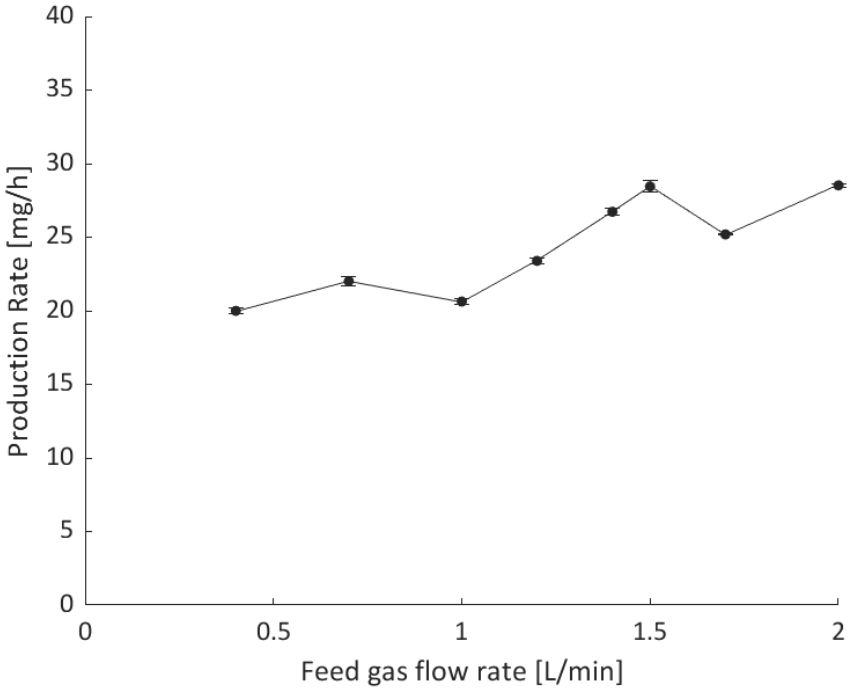

Fig. S.9 Production rate as a function of the feed gas flow rate.

S.3.2 Energy Transfer due to Electron Impact Reactions

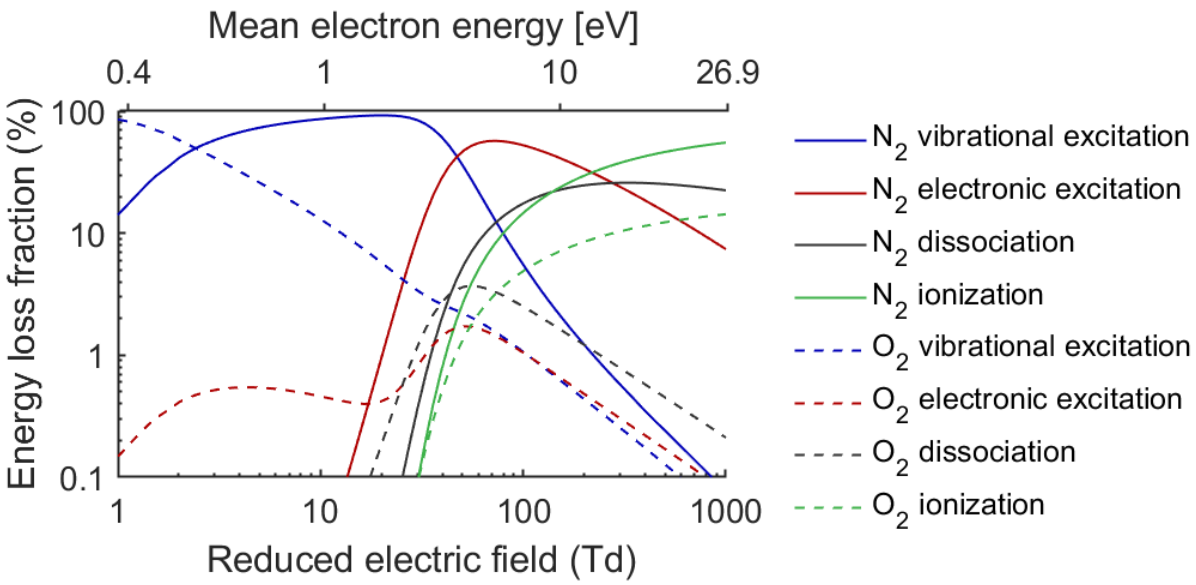

Fig. S.10 The electron energy loss to various electron impact processes as a function of the reduced electric field (bottom x-axis) and the mean electron energy (top x-axis) at 80/20 N_2/O_2 gas composition and 1750 K.

S.3.3 VDF of O_2

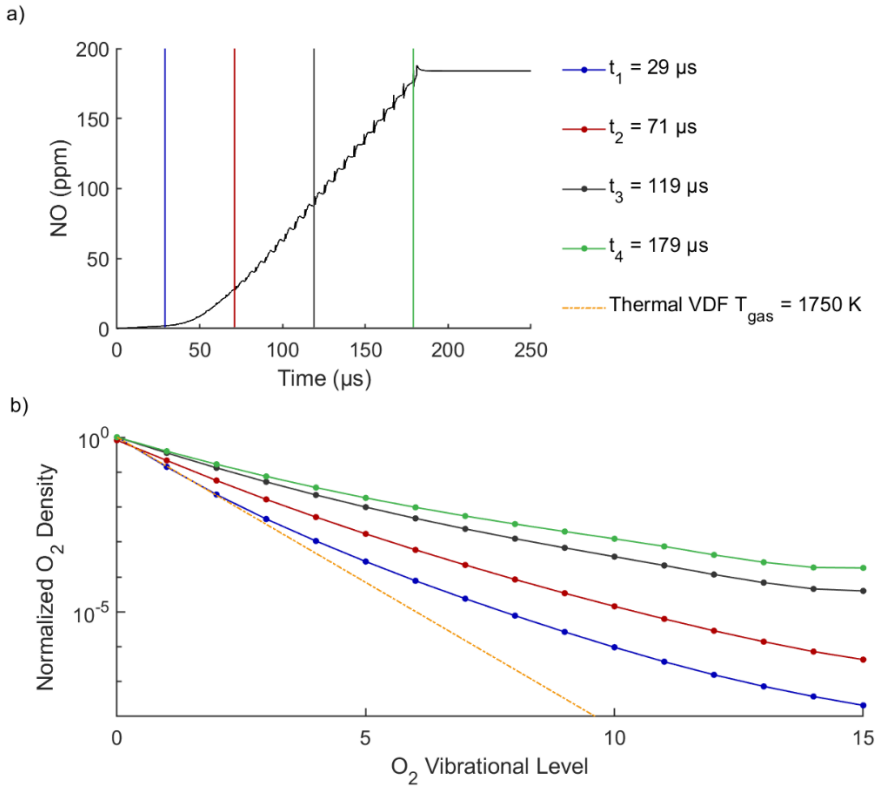

Fig. S.11 (a) Calculated NO concentration (black curve) as a function of time, during its residence time in the plasma (at 1 L/min), encountering a train of pulses, and (b) calculated VDF of O_2 taken in the middle of each pulse, for four different time points, as indicated by the vertical coloured lines in (a). The thermal VDF at 1750 K is also plotted.

S.3.4 Reaction analysis

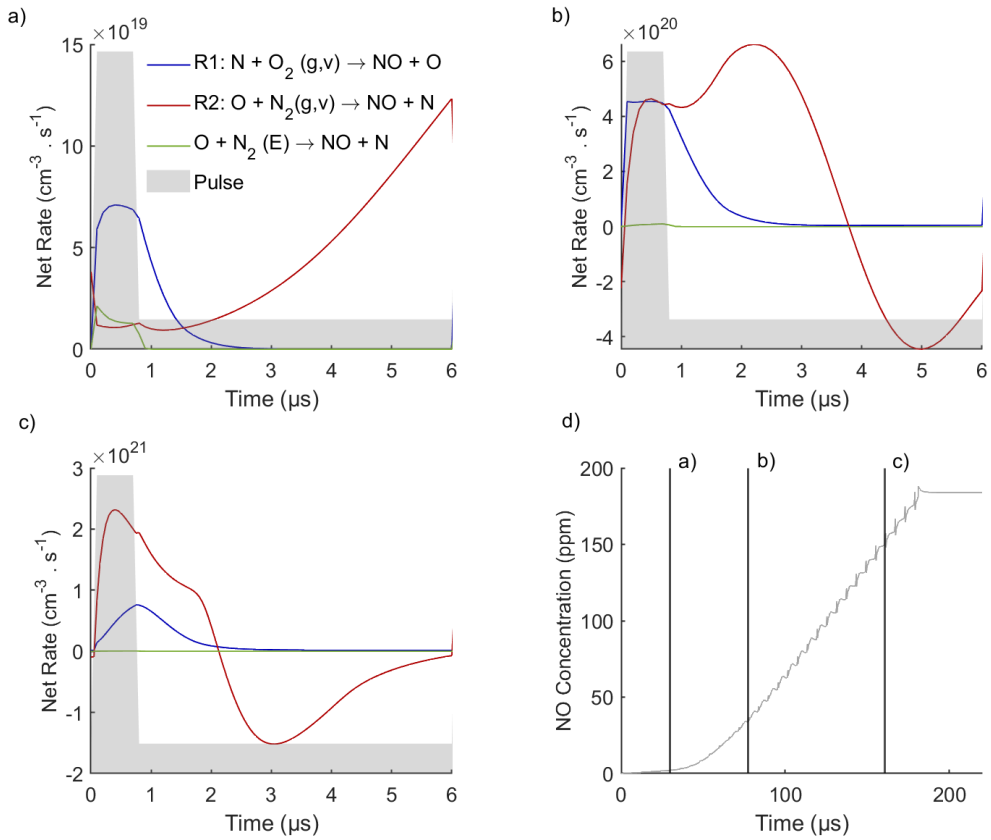

Fig. S.12 (a, b, c) Net reaction rates of the most important NO production reactions as a function of time during one pulse and interpulse time. A negative rate means that the reaction occurs in the opposite direction, i.e., as NO loss reaction. Panel (d) shows the time points in the pulse train, during the gas residence time in the plasma (at 1 L/min), with the associated NO concentration as a function of time: (a) Beginning, (b) middle, (c) end of the residence time. The x-axis of (a), (b) and (c) always starts at the beginning of a pulse.

We calculated the time- and space-averaged reaction rates for all formation and loss processes of NO and NO_2, as listed in **Table 3** of the main text. The results are plotted in **Fig. S.12**. Panels a, b and c present the reaction analysis of the main NO_x formation reactions as a function of time for one pulse – interpulse cycle, at the beginning, middle and end of the residence time in the plasma, as annotated by the three vertical lines in panel d. Throughout the whole residence time, the non-thermal Zeldovich mechanism promoted by vibrational excitation is the main mechanism for NO formation (blue and red curve; R1 and R2; see also **Table 3**). Note that the reactions with highest rate, overall, are the oxidation of NO to NO_2 (R3) and vice versa (R4),

which happen throughout the whole residence time and produce a limited amount of NO_2 (< 1 ppm at all investigated flow rates). However, they do not contribute to the initial NO_x formation, and are therefore not plotted in **Fig. S.12**. In the following, we describe the mechanism in more detail.

(a) In the beginning, there are only small amounts of reactive species (N and O atoms, and N_2 and O_2 vibrationally excited levels) present, so the first pulses are predominantly governed by the temperature dependence of the reaction rate constants (k). Note that for this reason the net reaction rates increase overall with residence time in the plasma (from a → b → c), as reactive species densities increase but the temperature remains constant. The rate of R1 (**Fig. S.12**; blue curve) is higher than for R2 (red curve) during the pulse, because its rate constant is higher at higher temperature (hence in the pulse), and it drops after the pulse, due to the drop in temperature. At the same time, the rate of R2 rises, due to the rising population of N_2 vibrationally excited states during the interpulse.
At short residence times, R2 from N_2(E) (green curve) also plays a small role. Its contribution drastically reduces compared to the vibrationally promoted reactions, as the population of the vibrational states increases throughout the residence time, while the population of N_2(E) does not.

(b, c) At longer residence time, the gas mixture contains a significant amount of N and O atoms, as well as vibrationally excited N_2 and O_2 molecules, and this affects the reaction behaviour.
(b) R1 still reaches its maximum rate during the pulse and slowly drops after the pulse. The maximum is clearly higher, because the N atoms are abundant now, and the reaction is not limited anymore by the energy-intensive splitting of N_2 (to produce N atoms), due to the strong V-T non-equilibrium. On the other hand, the rate of R2 first increases and then drops below 0 from the middle till the end of the interpulse. Indeed, during the first part of the interpulse, the O atom density is still high and the N_2(v) density increases. However, after 2 µs, the back reaction of R2 becomes more and more important compared to the forward reaction, so around 3.8 µs, there is net destruction of NO via L2. Indeed, the rate coefficient of this back reaction is temperature-independent, while the rate coefficient of the forward reaction decreases due to the lower temperatures. This back reaction was not yet important in the beginning (**Fig. S.12**), because of the low concentration of N atoms at that stage.

(c) At the end of the residence time, R2 is now the dominant reaction in the pulse due to the high density of higher vibrationally excited N_2. The maximum rate of R1 has moved to the end of the pulse. Indeed, R1 relies on R2 for the production of N atoms, so its maximum is reached after the maximum of R2. As R1 cannot compete anymore for the N atoms at low temperature (low k), the rate of L1 increases earlier in the interpulse. As the O atoms are thus consumed by L1, there is no maximum for R2, and its net rate gradually decreases until it becomes negative (net loss of NO).
Both in (b) and (c) the destruction of NO diminishes near the end of the interpulse (red curve returns to 0), due to the increasing population of $N_2(v)$ throughout the interpulse.

S.3.5 Reaction Rate Constants of the Zeldovich Mechanism

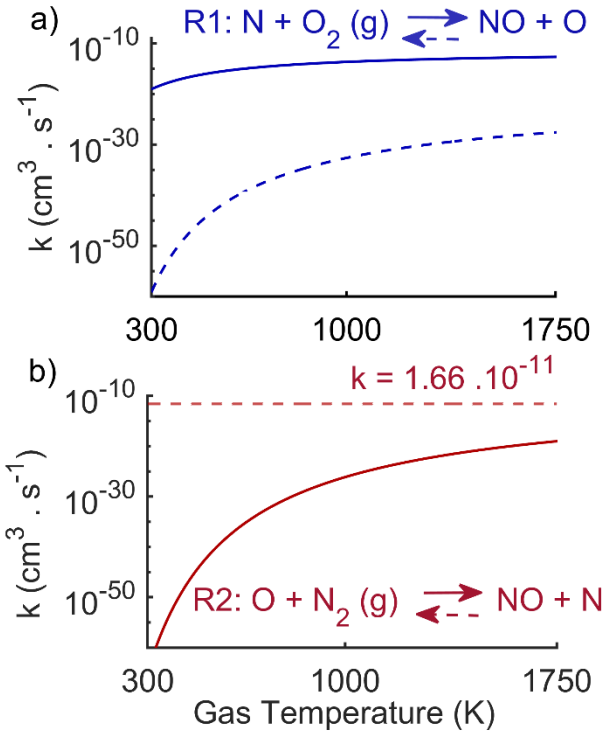

Figure S.13 Reaction rate constants (k) for the forward (full) and backward (dashed) reaction of (a) R1 and (b) R2, as a function of gas temperature. Note the y-axes on both panels are on a log scale.

APPENDIX

Table S.1 Electron impact reactions implemented in the model for atomic and molecular nitrogen and oxygen species as well as NO_x species. The list includes vibrational excitation and de-excitation, electronic excitation and de-excitation, direct and dissociative ionization, dissociation, and direct and dissociative attachment reactions. When the rate coefficient is not specified, these reactions are treated by energy-dependent cross sections. The rate coefficients are expressed in $cm^3\ s^{-1}$ or $cm^6\ s^{-1}$ for binary or ternary reactions, respectively.

Reaction	Rate Coefficient	Ref.	Note
$e^- + N_2 \leftrightarrow e^- + N_2(v)$		14	
$e^- + N_2(v) \leftrightarrow e^- + N_2(v')$		14	
$e^- + N_2(g,v) \rightarrow e^- + N_2(E_x)$		15	a, b, c
$e^- + N_2(E_x) \rightarrow e^- + N_2$		15	b
$e^- + N_2(g,v) \rightarrow 2e^- + N_2^+$		16	a
$e^- + N_2(E_x) \rightarrow 2e^- + N_2^+$		16	b,c
$e^- + N \rightarrow 2e^- + N^+$		15	
$e^- + N_2(g,v) \rightarrow 2e^- + N^+ + N$		17	a
$e^- + N_2(g,v) \rightarrow e^- + N + N$		15	a, c
$e^- + N_2(E_x) \rightarrow e^- + N + N$		15	b, c
$e^- + N \rightarrow e^- + N(E_x)$		15	d
$e^- + O_2 \leftrightarrow e^- + O_2(v)$		14	
$e^- + O_2(v) \leftrightarrow e^- + O_2(v')$		18	
$e^- + O_2(g,v) \rightarrow e^- + O_2(E_x)$		15	a, c, e
$e^- + O_2(E_x) \rightarrow e^- + O_2$		15	e
$e^- + O_2(g,v) \rightarrow 2e^- + O_2^+$		16	a, c
$e^- + O_2(E_x) \rightarrow 2e^- + O_2^+$		19	e, c
$e^- + O \rightarrow 2e^- + O^+$		15	
$e^- + O_2(g,v) \rightarrow 2e^- + O + O^+$		20	a, c
$e^- + O_2(E_x) \rightarrow 2e^- + O + O^+$		20	e,c
$e^- + O_3 \rightarrow 2e^- + O + O_2^+$		21	

$e^- + O_3 \rightarrow e^- + O^+ + O^- + O$		15	
$e^- + O_2(g,v) \rightarrow e^- + O + O$		15	a
$e^- + O_3 \rightarrow e^- + O_2 + O$		21	
$e^- + O_2(g,v) \rightarrow O + O^-$		15	a, c
$e^- + O_2(g,v) + M \rightarrow O_2^- + M$		22	a, c, f
$e^- + O_3 \rightarrow O^- + O_2$		16	
$e^- + O_3 \rightarrow O + O_2^-$		16	
$e^- + O_3 + M \rightarrow O_3^- + M$	5×10^{-31}	23	f
$e^- + O + M \rightarrow O^- + M$	1×10^{-31}	24	f
$e^- + NO \rightarrow 2e^- + NO^+$		17	
$e^- + NO_2 \rightarrow 2e^- + NO_2^+$		25	
$e^- + N_2O \rightarrow 2e^- + N_2O^+$		26	
$e^- + N_2O \rightarrow e^- + N_2 + O$		27	
$e^- + N_2O \rightarrow e^- + N_2 + O(1D)$		27	
$e^- + N_2O \rightarrow e^- + NO + N$		27	
$e^- + NO \rightarrow O^- + N$		17	
$e^- + N_2O \rightarrow N_2 + O^-$		26	
$e^- + NO_2 \rightarrow NO_2^-$	1×10^{-11}	28	
$e^- + NO_2 \rightarrow O^- + NO$	1×10^{-11}	29	
$e^- + NO + M \rightarrow NO^- + M$	8×10^{-31}	29	f
$e^- + N_2O + M \rightarrow N_2O^- + M$	6×10^{-33}	29	f

[a] For any species indicated with (g,v), g and v stand for its ground and vibrationally excited state, respectively.

[b] $N_2(E_x)$ represents the electronically excited states: $N_2(A^3\Sigma_u^+)$, $N_2(B^3\Pi_g)$, $N_2(C^3\Pi_u)$ and $N_2\left(a'^1\Sigma_u^-\right)$.

[c] The cross sections of the reactions involving excited species on the left hand side are shifted over the difference in the threshold energies.

[d] $N(E_x)$ represents the electronically excited states of atomic N: $N(2D)$ and $N(2P)$.

[e] $O_2(E_x)$ represents the electronically excited states: $O_2(a^1\Delta)$, $O_2(b^1\Sigma^+)$ and a combination of three states, i.e. $O_2(A^3\Sigma^+, C^3\Delta, c^1\Sigma^-)$ at a threshold energy of 4.5 eV.

[f] M represents any neutral molecule.

Table S.2 Neutral-neutral reactions included in the model and the corresponding rate coefficient expressions. T_g is the gas temperature in Kelvin. The rate coefficients are expressed in $cm^3\ s^{-1}$ or $cm^6\ s^{-1}$ for binary or ternary reactions, respectively. For certain reactions, the rate coefficients of the vibrationally excited species are determined according to the Fridman-Macheret model in which the activation energy is reduced by $\alpha\ E_v$, where α is the vibrational efficiency to lower the activation barrier and E_v is the vibrational energy. For those reactions, the α parameter is given in the last column.

Reaction	Rate coefficient	Ref.	Note
$N_2(g,v) + M \rightarrow N + N + M$	$8.37 \times 10^{-4} \times \left(\frac{T_g}{298}\right)^{-3.5} \times \exp\left(-\frac{113710}{T_g}\right)$	30	a, b $\alpha = 1$
$N + N + M \rightarrow N_2 + M$	$1.38 \times 10^{-33} \times \exp\left(\frac{502.978}{T_g}\right)$	31	b
$N + N \rightarrow N_2^+ + e^-$	$2.7 \times 10^{-11} \times \exp\left(-\frac{6.74\times10^4}{T_g}\right)$	29	
$N + N + N \rightarrow N_2(A^3\Sigma_u^+) + N$	1.0×10^{-32}	29	
$N + N + N \rightarrow N_2(B^3\Pi_g) + N$	1.4×10^{-32}	29	
$N + N + N_2 \rightarrow N_2(A^3\Sigma_u^+) + N_2$	1.7×10^{-33}	29	
$N + N + N_2 \rightarrow N_2(B^3\Pi_g) + N_2$	2.4×10^{-33}	29	
$N(2D) + M \rightarrow N + M$	2.4×10^{-14}	32	b
$N(2P) + N \rightarrow N(2D) + N$	1.8×10^{-12}	29	
$N(2P) + N_2 \rightarrow N + N_2$	2.0×10^{-18}	29	
$N_2\left(a'^1\Sigma_u^-\right) + N \rightarrow N_2 + N$	2.0×10^{-11}	32	
$N_2\left(a'^1\Sigma_u^-\right) + N_2 \rightarrow N_2 + N_2$	3.7×10^{-16}	32	
$N_2\left(a'^1\Sigma_u^-\right) + N_2 \rightarrow N_2(B^3\Pi_g) + N_2$	1.9×10^{-13}	29	
$N_2\left(a'^1\Sigma_u^-\right) + N_2\left(a'^1\Sigma_u^-\right) \rightarrow N_2^+ + N_2 + e^-$	5.0×10^{-13}	32	
$N_2\left(a'^1\Sigma_u^-\right) + N_2\left(a'^1\Sigma_u^-\right) \rightarrow N_4^+ + e^-$	1.0×10^{-11}	29	

$N_2\left(a'^1\Sigma_u^-\right) + N_2(A^3\Sigma_u^+) \rightarrow N_4^+ + e^-$	4.0×10^{-12}	29	
$N_2(A^3\Sigma_u^+) + N \rightarrow N_2 + N(2P)$	$4.0 \times 10^{-11} \times \left(\frac{300}{T_g}\right)^{0.667}$	29	
$N_2(A^3\Sigma_u^+) + N \rightarrow N_2 + N$	2.0×10^{-12}	29	
$N_2(A^3\Sigma_u^+) + N_2 \rightarrow N_2 + N_2$	3.0×10^{-16}	29	
$N_2(A^3\Sigma_u^+) + N_2\left(a'^1\Sigma_u^-\right) \rightarrow N_2^+ + N_2 + e^-$	1.0×10^{-12}	32	
$N_2(A^3\Sigma_u^+) + N_2(A^3\Sigma_u^+) \rightarrow N_2 + N_2(A^3\Sigma_u^+)$	2.0×10^{-12}	32	
$N_2(A^3\Sigma_u^+) + N_2(A^3\Sigma_u^+) \rightarrow N_2 + N_2\left(B^3\Pi_g\right)$	3.0×10^{-10}	29	
$N_2(A^3\Sigma_u^+) + N_2(A^3\Sigma_u^+) \rightarrow N_2 + N_2(C^3\Pi_u)$	1.5×10^{-10}	29	
$N_2\left(B^3\Pi_g\right) + N_2 \rightarrow N_2 + N_2$	2.0×10^{-12}	29	
$N_2\left(B^3\Pi_g\right) + N_2 \rightarrow N_2(A^3\Sigma_u^+) + N_2$	3×10^{-11}	29	
$N_2(C^3\Pi_u) + N_2 \rightarrow N_2 + \left(a'^1\Sigma_u^-\right)$	1.0×10^{-11}	29	
$O_2(g, v) + M \rightarrow O + O + M$	$\left(\frac{3.0\times10^{-6}}{T_g}\right) \times \exp\left(\frac{-59380}{T_g}\right)$		a $\alpha = 1$
$O + O + M \rightarrow O_2 + M$	$5.21 \times 10^{-35} \times \exp\left(\frac{900}{T_g}\right)$	33	b
$O + O_3 \rightarrow O_2 + O_2$	$8.0 \times 10^{-12} \times \exp\left(-\frac{2056}{T_g}\right)$	34	
$O + O_2(g, v) + M \rightarrow O_3 + M$	$1.34 \times 10^{-34} \times \left(\frac{T_g}{298}\right)^{-1.0}$	35	a, b
$O_3 + M \rightarrow O_2 + O + M$	$7.16 \times 10^{-10} \times \exp\left(-\frac{98120}{R_g T_g}\right)$	36	b, c
$O + O_2(E_x) + M \rightarrow O_3 + M$	$1.34 \times 10^{-34} \times \left(\frac{T_g}{298}\right)^{-1.0}$	35	b, d, e
$O + O_3 \rightarrow O_2 + O_2(a^1\Delta)$	$2.0 \times 10^{-11} \times \exp\left(-\frac{2280}{T_g}\right)$	29	
$O_2(a^1\Delta) + O \rightarrow O_2 + O$	7.0×10^{-16}	29	

$O_2(a^1\Delta) + O_2 \rightarrow O_2 + O_2$	$3.8 \times 10^{-18} \times \exp\left(-\frac{205}{T_g}\right)$	29	
$O_2(b^1\Sigma^+) + O \rightarrow O_2(a^1\Delta) + O$	8.1×10^{-14}	29	
$O_2(b^1\Sigma^+) + O \rightarrow O_2 + O(1D)$	$3.4 \times 10^{-11} \times \left(\frac{T_g}{300}\right)^{-0.1} \times \exp\left(-\frac{4200}{T_g}\right)$	29	
$O_2(b^1\Sigma^+) + O_2 \rightarrow O_2 + O_2(a^1\Delta)$	$4.3 \times 10^{-22} \times (T_g)^{2.4} \times \exp\left(-\frac{281}{T_g}\right)$	29	
$O_2(b^1\Sigma^+) + O_3 \rightarrow O_2 + O_2 + O$	2.2×10^{-11}	29	
$O_2(a^1\Delta) + O_3 \rightarrow O_2 + O_2 + O(1D)$	$5.2 \times 10^{-11} \times \exp\left(-\frac{2840}{T_g}\right)$	29	
$O_2(a^1\Delta) + O_2(a^1\Delta) \rightarrow O_2 + O_2(b^1\Sigma^+)$	$7.0 \times 10^{-28} \times (T_g)^{3.8} \times \exp\left(\frac{700}{T_g}\right)$	29	
$O(1D) + O \rightarrow O + O$	8.0×10^{-12}	29	
$O(1D) + O_2 \rightarrow O + O_2$	$6.4 \times 10^{-12} \times \exp\left(-\frac{67}{T_g}\right)$	29	
$O(1S) + O \rightarrow O(1D) + O(1D)$	$5.0 \times 10^{-11} \times \exp\left(-\frac{300}{T_g}\right)$	29	
$O(1S) + O_2 \rightarrow O + O_2$	$1.3 \times 10^{-12} \times \exp\left(-\frac{850}{T_g}\right)$	29	
$O(1S) + O_2 \rightarrow O + O + O$	3.0×10^{-12}	29	
$O(1S) + O_2(a^1\Delta) \rightarrow O + O + O$	3.2×10^{-11}	29	
$O(1S) + O_2(a^1\Delta) \rightarrow O(1D) + O_2(b^1\Sigma^+)$	2.9×10^{-11}	29	
$O(1S) + O_2 \rightarrow O + O_2(A^3\Sigma^+, C^3\Delta, c^1\Sigma^-)$	$3.0 \times 10^{-12} \times \exp\left(-\frac{850}{T_g}\right)$	29	f
$N + O_2(g, v) \rightarrow O + NO$	$2.36 \times 10^{-11} \times \exp\left(-\frac{44230}{R_g T_g}\right)$	37	a, c $\alpha = 0.24$
$O + N_2(g, v) \rightarrow N + NO$	$3.01 \times 10^{-10} \times \exp\left(-\frac{318000}{R_g T_g}\right)$	38	a, c $\alpha = 1$

$O_3 + N \rightarrow NO + O_2$	$5.0 \times 10^{-12} \times \exp\left(-\frac{650}{T_g}\right)$	34	
$O_3 + NO \rightarrow O_2 + NO_2$	$2.5 \times 10^{-13} \times \exp\left(-\frac{765}{T_g}\right)$	29	
$O_3 + NO_2 \rightarrow O_2 + NO_3$	$1.2 \times 10^{-13} \times \exp\left(-\frac{2450}{T_g}\right)$	28	
$NO_3 + O_3 \rightarrow NO_2 + O_2 + O_2$	1.0×10^{-17}	39	
$N + NO \rightarrow O + N_2$	1.66×10^{-11}	40	
$N + NO_2 \rightarrow O + O + N_2$	9.1×10^{-13}	29	
$N + NO_2 \rightarrow O + N_2O$	3.0×10^{-12}	29	
$N + NO_2 \rightarrow N_2 + O_2$	7.0×10^{-13}	29	
$N + NO_2 \rightarrow NO + NO$	2.3×10^{-12}	29	
$O + NO \rightarrow N + O_2$	$7.5 \times 10^{-12} \times \left(\frac{T_g}{300}\right) \times \exp\left(-\frac{19500}{T_g}\right)$	29	
$\mathbf{O + NO_2 \rightarrow NO + O_2}$	$\mathbf{5.5 \times 10^{-12} \times \exp(\frac{188}{T_g})}$	41	**i**
$O + N_2O \rightarrow NO + NO$	$1.5 \times 10^{-10} \times \exp\left(-\frac{14090}{T_g}\right)$	29	
$O + N_2O \rightarrow N_2 + O_2$	$8.3 \times 10^{-12} \times \exp\left(-\frac{14000}{T_g}\right)$	29	
$O + NO_3 \rightarrow O_2 + N_2$	1.0×10^{-11}	29	
$NO + NO \rightarrow N + NO_2$	$3.3 \times 10^{-16} \times \left(\frac{300}{T_g}\right)^{0.5} \times \exp\left(-\frac{39200}{T_g}\right)$	29	
$NO + NO \rightarrow O + N_2O$	$2.2 \times 10^{-12} \times \exp\left(-\frac{32100}{T_g}\right)$	29	
$NO + NO \rightarrow N_2 + O_2$	$5.1 \times 10^{-13} \times \exp\left(-\frac{33660}{T_g}\right)$	29	
$NO + N_2O \rightarrow N_2 + NO_2$	$4.6 \times 10^{-10} \times \exp\left(-\frac{25170}{T_g}\right)$	29	
$NO + NO_3 \rightarrow NO_2 + NO_2$	1.7×10^{-11}	29	
$NO_2 + NO_2 \rightarrow NO + NO_3$	$4.5 \times 10^{-10} \times \exp\left(-\frac{18500}{T_g}\right)$	29	

$NO_2 + NO_2 \rightarrow NO + NO + O_2$	$3.3 \times 10^{-12} \times \exp\left(-\frac{13500}{T_g}\right)$	[29]	
$NO_2 + NO_3 \rightarrow NO + NO_2 + O_2$	$2.3 \times 10^{-13} \times \exp\left(-\frac{1600}{T_g}\right)$	[29]	
$NO_3 + NO_3 \rightarrow O_2 + NO_2 + NO_2$	$4.3 \times 10^{-12} \times \exp\left(-\frac{3850}{T_g}\right)$	[29]	
$NO + O_2(g,v) \rightarrow O + NO_2$	$2.8 \times 10^{-12} \times \exp\left(-\frac{23400}{T_g}\right)$	[29]	a $\alpha = 1$
$NO + NO + O_2(g,v) \rightarrow NO_2 + NO_2$	$3.3 \times 10^{-39} \times \exp\left(-\frac{4410}{R_g T_g}\right)$	[42]	a, c $\alpha =$ 0.2
$NO_2 + O_2(g,v) \rightarrow NO + O_3$	$2.8 \times 10^{-12} \times \exp\left(-\frac{25400}{T_g}\right)$	[29]	a $\alpha =$ 0.2
$NO_3 + O_2(g,v) \rightarrow O_3 + NO_2$	$1.5 \times 10^{-12} \times \exp\left(-\frac{15020}{T_g}\right)$	[29]	a $\alpha =$ 0.8
$NO + O \rightarrow NO_2$	$3.01 \times 10^{-11} \times \left(\frac{T_g}{300}\right)^{-0.75}$	[43]	
$NO_2 + NO + M \rightarrow N_2O_3 + M$	$3.09 \times 10^{-34} \times \left(\frac{T_g}{300}\right)^{-7.70}$	[34]	b
$NO_2 + NO_2 + M \rightarrow N_2O_4 + M$	$1.4 \times 10^{-33} \times \left(\frac{T_g}{300}\right)^{-3.8}$	[34]	b
$NO_2 + NO_3 + M \rightarrow N_2O_5 + M$	$3.7 \times 10^{-30} \times \left(\frac{300}{T_g}\right)^{4.10}$	[42]	b
$N + O + M \rightarrow NO + M$	$1.0 \times 10^{-32} \times \left(\frac{300}{T_g}\right)^{0.5}$	[29]	b
$N_2(g,v) + O + M \rightarrow N_2O + M$	$3.9 \times 10^{-35} \times \exp\left(-\frac{10400}{T_g}\right)$	[29]	b
$N_2O + M \rightarrow N_2 + O + M$	$1.20 \times 10^{-9} \times \exp\left(-\frac{240000}{R_g T_g}\right)$	[29]	b, c

$NO_2 + M \rightarrow NO + O + M$	$9.4 \times 10^{-5} \times \left(\frac{T_g}{298}\right)^{-2.66} \times \exp\left(-\frac{311000}{R_g T_g}\right)$	43	b, c
$NO_3 + M \rightarrow NO + O_2 + M$	$2.51 \times 10^{-14} \times \exp\left(-\frac{10230}{R_g T_g}\right)$	44	b, c
$NO + M \rightarrow N + O + M$	$8.7 \times 10^{-9} \times \exp\left(-\frac{75994}{T_g}\right)$	29	b
$N_2O_3 + M \rightarrow NO + NO_2 + M$	$1.91 \times 10^{-7} \times \left(\frac{T_g}{298}\right)^{-8.7} \times \exp\left(-\frac{40570}{R_g T_g}\right)$	34	b, c
$N_2O_4 + M \rightarrow NO_2 + NO_3 + M$	$1.3 \times 10^{-5} \times \left(\frac{T_g}{298}\right)^{-3.8} \times \exp\left(-\frac{53210}{R_g T_g}\right)$	34	b, c
$N_2O_5 + M \rightarrow NO_2 + NO_3 + M$	$2.1 \times 10^{-11} \times \left(\frac{300}{T_g}\right)^{-3.5} \times \exp\left(-\frac{91460}{R_g T_g}\right)$	29	b, c
$NO + O_2(g, v) + M \rightarrow NO_3 + M$	$5.65 \times 10^{-41} \times \exp\left(-\frac{1750}{R_g T_g}\right)$	45	a, b, c
$NO + O_2(E_x) + M \rightarrow NO_3 + M$	$5.65 \times 10^{-41} \times \exp\left(-\frac{1750}{R_g T_g}\right)$	45	b, d
$N + N + NO \rightarrow N_2(A^3\Sigma_u^+) + NO$	1.7×10^{-33}	29	
$N + N + NO \rightarrow N_2(B^3\Pi_g) + NO$	2.4×10^{-33}	29	
$N + N + O \rightarrow N_2(A^3\Sigma_u^+) + O$	1.0×10^{-32}	29	
$N + N + O \rightarrow N_2(B^3\Pi_g) + O$	1.4×10^{-32}	29	
$N + N + O_2 \rightarrow N_2(A^3\Sigma_u^+) + O_2$	1.7×10^{-33}	29	
$N + N + O_2 \rightarrow N_2(B^3\Pi_g) + O_2$	2.4×10^{-33}	29	
$N(2D) + N_2O \rightarrow NO + N_2$	3.5×10^{-12}	29	
$N(2D) + NO \rightarrow N_2 + O$	1.8×10^{-10}	29	
$N(2D) + O \rightarrow N + O(1D)$	4.0×10^{-13}	29	
$N(2D) + O_2(g, v) \rightarrow NO + O$	5.2×10^{-12}	29	a

$N(2P) + NO \rightarrow N_2(A^3\Sigma_u^+) + O$	3.0×10^{-11}	29	
$N(2P) + O \rightarrow N + O$	1.0×10^{-12}	29	
$N(2P) + O_2(g, v) \rightarrow NO + O$	2.6×10^{-15}	29	a
$N_2\left(a'^1\Sigma_u^-\right) + NO \rightarrow N_2 + N + O$	3.6×10^{-10}	29	
$N_2\left(a'^1\Sigma_u^-\right) + O \rightarrow NO + N$	3.0×10^{-10}	38	
$N_2\left(a'^1\Sigma_u^-\right) + O_2(g, v) \rightarrow N_2 + O + O$	2.8×10^{-11}	29	a
$N_2(A^3\Sigma_u^+) + N_2O \rightarrow N_2 + N + NO$	1.0×10^{-11}	29	
$N_2(A^3\Sigma_u^+) + NO \rightarrow N_2 + NO$	6.9×10^{-11}	29	
$N_2(A^3\Sigma_u^+) + NO_2 \rightarrow N_2 + O + NO$	1.0×10^{-12}	29	
$N_2(A^3\Sigma_u^+) + O \rightarrow N_2 + O(1S)$	2.1×10^{-11}	29	
$N_2(A^3\Sigma_u^+) + O \rightarrow NO + N(2D)$	7.0×10^{-12}	29	
$N_2(A^3\Sigma_u^+) + O_2(g, v) \rightarrow N_2 + O + O$	$2.0 \times 10^{-12} \times \left(\frac{T_g}{300}\right)^{0.55}$	29	a
$N_2(A^3\Sigma_u^+) + O_2 \rightarrow N_2 + O_2(a^1\Delta)$	$2.0 \times 10^{-13} \times \left(\frac{T_g}{300}\right)^{0.55}$	29	
$N_2(A^3\Sigma_u^+) + O_2 \rightarrow N_2 + O_2$	2.54×10^{-12}	29	
$N_2(A^3\Sigma_u^+) + O_2(g, v) \rightarrow N_2O + O$	$2.0 \times 10^{-14} \times \left(\frac{T_g}{300}\right)^{0.55}$	29	a
$N_2\left(B^3\Pi_g\right) + N_2O \rightarrow N_2 + N + NO$	0.58×10^{-10}	46	
$N_2\left(B^3\Pi_g\right) + N_2O \rightarrow N_2 + N_2 + O$	0.58×10^{-10}	46	
$N_2\left(B^3\Pi_g\right) + O \rightarrow NO + N$	3.0×10^{-10}	38	
$N_2(C^3\Pi_u) + O \rightarrow NO + N$	3.0×10^{-10}	38	
$N_2(C^3\Pi_u) + O_2(g, v) \rightarrow N_2 + O + O$	3.0×10^{-10}	29	a
$NO + O_2(E_x) \rightarrow O + NO_2$	$2.8 \times 10^{-12} \times \exp\left(-\frac{23400}{T_g}\right)$	29	d, g
$NO_3 + O_2(E_x) \rightarrow O_3 + NO_2$	$1.5 \times 10^{-12} \times \exp\left(-\frac{15020}{T_g}\right)$	29	d, h
$O(1D) + N_2 \rightarrow N_2 + O$	2.3×10^{-11}	29	

$O(1S) + N \rightarrow O + N$	1.0×10^{-12}	[29]	
$O(1S) + N_2(g, v) \rightarrow O + N_2(g, v)$	1.0×10^{-17}	[29]	
$O_2(a^1\Delta) + N \rightarrow NO + O$	$2.0 \times 10^{-14} \times \exp\left(-\frac{600}{T_g}\right)$	[29]	
$O_2(a^1\Delta) + N_2(g, v) \rightarrow O_2 + N_2(g, v)$	3.0×10^{-21}	[29]	
$O_2(a^1\Delta) + NO \rightarrow O_2 + NO$	2.5×10^{-11}	[29]	
$O_2(b^1\Sigma^+) + N_2 \rightarrow O_2(a^1\Delta) + N_2$	$1.7 \times 10^{-15} \times \left(\frac{T_g}{300}\right)^{1.0}$	[29]	
$N_2(B^3\Pi_g) + NO \rightarrow N_2(A^3\Sigma_u^+) + NO$	2.4×10^{-10}	[29]	
$N_2(B^3\Pi_g) + O_2(g, v) \rightarrow N_2 + O + O$	3.0×10^{-10}	[29]	a

[a] For any species indicated with (g, v), g and v stand for its ground and vibrationally excited state, respectively.

[b] M represents any neutral molecule.

[c] $R_g = 8.3144598\ J.K^{-1}.mol^{-1}$ is the universal gas constant.

[d] $O_2(E_x)$ represents the two electronically excited states: $O_2(a^1\Delta)$ and $O_2(b^1\Sigma^+)$.

[e] The rate coefficient is assumed to be equal to that of $O + O_2 + M \rightarrow O_3 + M$.

[f] $O_2(A^3\ \Sigma^+, C^3\ \Delta, c^1\ \Sigma^-)$ is a combination of three electronic excited states at a threshold energy of 4.5 eV.

[g] The rate coefficient is assumed to be equal to that of $NO + O_2 \rightarrow O + NO_2$.

[h] The rate coefficient is assumed to be equal to that of $NO_3 + O_2 \rightarrow O_3 + NO_2$.

The reaction rate coefficient for this reaction has been changed compared to our previous work. Before k = $9.05 \times 10^{-12} \times \left(\frac{T_g}{298}\right)^{-0.52}$ from [41] was used. The updated reaction rate coefficient was found to be more appropriate after critical review of the literature.

Table S.3 Electron-ion recombination reactions included in the model and the corresponding rate coefficient expressions. T_e is to the electron temperature in K and T_g is the gas temperature in K. The rate coefficients are expressed in $cm^3\ s^{-1}$ or $cm^6\ s^{-1}$ for binary or ternary reactions, respectively.

Reaction	Rate coefficient	Ref.	Note
$e^- + N_2^+ \rightarrow N + N(g, E_x)$	$R \times 1.8 \times 10^{-7} \times \left(\frac{300}{T_e}\right)^{0.39}$	29	a
$e^- + N_3^+ \rightarrow N_2 + N$	$2 \times 10^{-7} \times \left(\frac{300}{T_e}\right)^{0.5}$	47	
$e^- + N_3^+ \rightarrow N_2(E_x) + N$	$6.91 \times 10^{-8} \times \left(\frac{T_e}{11604.5}\right)^{-0.5}$	47	c
$e^- + N_4^+ \rightarrow N_2 + N_2$	$2.3 \times 10^{-6} \times \left(\frac{300}{T_e}\right)^{0.53}$	29	
$e^- + N_4^+ \rightarrow N_2 + N + N$	$3.13 \times 10^{-7} \times \left(\frac{T_e}{11604.5}\right)^{-0.41}$	47	
$e^- + N^+ + e^- \rightarrow e^- + N$	$7 \times 10^{-20} \times \left(\frac{300}{T_e}\right)^{4.5}$	47	
$e^- + N^+ + M \rightarrow N + M$	$6 \times 10^{-27} \times \left(\frac{300}{T_e}\right)^{1.5}$	48	b
$e^- + N_2^+ + e^- \rightarrow e^- + N_2$	$1 \times 10^{-19} \times \left(\frac{T_e}{300}\right)^{-4.5}$	47	
$e^- + N_2^+ + M \rightarrow N_2 + M$	$2.49 \times 10^{-29} \times \left(\frac{T_e}{11604.5}\right)^{-1.5}$	47	b
$e^- + O^+ + O_2 \rightarrow O + O_2$	$6 \times 10^{-27} \times \left(\frac{300}{T_e}\right)^{1.5}$	48	
$e^- + O^+ + e^- \rightarrow e^- + O$	$7 \cdot 10^{-20} \cdot \left(\frac{300}{T_e}\right)^{4.5}$	29	
$e^- + O_2^+ + M \rightarrow O_2 + M$	1×10^{-26}	24	b
$e^- + O_2^+ + e^- \rightarrow e^- + O_2$	$1 \times 10^{-19} \times \left(\frac{T_e}{300}\right)^{-4.5}$	48	
$e^- + O_2^+ \rightarrow O + O$	$6.46 \times 10^{-5} \times T_e^{-0.5} \times T_g^{-0.5}$	49	
$e^- + O_2^+ \rightarrow O + O(1D)$	$1.08 \times 10^{-7} \left(\frac{T_e}{300}\right)^{-0.7}$	29	
$e^- + O_2^+ \rightarrow O + O(1S)$	$0.14 \times 10^{-7} \left(\frac{T_e}{300}\right)^{-0.7}$	29	
$e^- + O_4^+ \rightarrow O_2 + O_2$	$1.4 \times 10^{-6} \times \left(\frac{300}{T_e}\right)^{0.5}$	29	

$e^- + NO^+ + e^- \rightarrow e^- + NO$	$1.0 \times 10^{-19} \left(\frac{T_e}{300}\right)^{-4.5}$	48	
$e^- + NO^+ + M \rightarrow NO + M$	$2.49 \times 10^{-29} \times \left(\frac{T_e}{11604.5}\right)^{-1.5}$	47	b
$e^- + NO^+ \rightarrow O + N(g, E_x)$	$R \times 4.2 \times 10^{-7} \times \left(\frac{300}{T_e}\right)^{0.85}$	29	d
$e^- + N_2O^+ \rightarrow N_2 + O$	$2.0 \times 10^{-7} \times \left(\frac{300}{T_e}\right)^{0.5}$	29	
$e^- + NO_2^+ \rightarrow NO + O$	$2.0 \times 10^{-7} \times \left(\frac{300}{T_e}\right)^{0.5}$	29	
$e^- + O_2^+N_2 \rightarrow O_2 + N_2$	$1.3 \times 10^{-6} \times \left(\frac{300}{T_e}\right)^{0.5}$	29	

[a] In $N(g, E_x)$, g stands for the ground state of atomic N and E_x represents two of its electronically excited states: $N(2D)$ and $N(2P)$; R is equal to 0.5, 0.45 and 0.05 for N, $N(2D)$ and $N(2P)$, respectively.
[b] M represents any neutral molecule.
[c] $N_2(E_x)$ represents $N_2(A^3\Sigma_u^+)$ and $N_2(B^3\Pi_g)$.
[d] In $N(g, E_x)$, g stands for the ground state of atomic N and E_x represents the electronic excited state $N(2D)$; R is equal to 0.2 and 0.8 for N and $N(2D)$, respectively.

Table S.4 Ion-neutral reactions included in the model and the corresponding rate coefficient expressions. T_g is the gas temperature in K. For certain reactions, T_{ion} is the effective temperature of the reacting ion in K. The calculations for T_{ion} can be found in [50]. The rate coefficients are expressed in $cm^3\ s^{-1}$ or $cm^6\ s^{-1}$ for binary or ternary reactions, respectively.

Reaction	Rate coefficient	Ref.	Note
$N_2^+ + N \rightarrow N^+ + N_2$	$7.2 \times 10^{-13} \times \left(\frac{T_{ion}}{300}\right)$	29	
$N_2^+ + N + N_2 \rightarrow N_3^+ + N_2$	$9.0 \times 10^{-30} \times \left(\frac{400}{T_{ion}}\right)$	29	
$N_4^+ + N_2 \rightarrow N_2^+ + N_2 + N_2$	$2.1 \times 10^{-16} \times \left(\frac{Tion}{121}\right)$	29	
$N^+ + N_2 + N_2 \rightarrow N_3^+ + N_2$	$1.7 \times 10^{-29} \times \left(\frac{300}{Tion}\right)^{2.1}$	29	
$N_2^+ + N_2 + N_2 \rightarrow N_4^+ + N_2$	$5.2 \times 10^{-29} \times \left(\frac{300}{T_{ion}}\right)^{2.2}$	29	
$N^+ + N + N_2 \rightarrow N_2^+ + N_2$	1.0×10^{-29}	29	

$N^+ + N \rightarrow N_2^+$	1.0×10^{-29}	[51]	
$N_3^+ + N \rightarrow N_2^+ + N_2$	6.6×10^{-11}	[29]	
$N_4^+ + N \rightarrow N^+ + N_2 + N_2$	1.0×10^{-11}	[29]	
$N_2^+ + N_2(A^3\Sigma_u^+) \rightarrow N_3^+ + N$	3.0×10^{-10}	[28]	
$O^- + M \rightarrow O + M + e^-$	4.0×10^{-12}	[28]	a
$O^- + O \rightarrow O_2 + e^-$	2.3×10^{-10}	[52]	
$O^- + O_2(g,v) + M \rightarrow O_3^- + M$	$1.1 \times 10^{-30} \times \exp\left(\frac{300}{T_g}\right)$	[52]	a, b
$O^- + O_2(g,v) \rightarrow O_3 + e^-$	5.0×10^{-15}	[29]	b
$O^- + O_3 \rightarrow O_2 + O_2 + e^-$	3.0×10^{-10}	[53]	
$O^- + O_3 \rightarrow O_3^- + O$	5.3×10^{-10}	[54]	
$O^+ + O + M \rightarrow O_2^+ + M$	1.0×10^{-29}	[48]	a
$O^+ + O_2(g,v) \rightarrow O + O_2^+$	$1.9 \times 10^{-11} \times \left(\frac{T_g}{300}\right)^{-0.5}$	[55]	b
$O^+ + O_3 \rightarrow O_2^+ + O_2$	1.0×10^{-10}	[48]	
$O_2^- + M \rightarrow O_2 + M + e^-$	$2.7 \times 10^{-10} \times \left(\frac{T_g}{300}\right)^{0.5} \times \exp\left(-\frac{5590}{T_g}\right)$	[55]	a
$O_2^- + O \rightarrow O_2 + O^-$	3.31×10^{-10}	[52]	
$O_2^- + O_2(g,v) + M \rightarrow O_4^- + M$	$3.5 \times 10^{-31} \times \left(\frac{T_g}{300}\right)^{-1.0}$	[48,52,54]	a, b
$O_2^- + O_2 \rightarrow O_2 + O_2 + e^-$	2.18×10^{-18}	[56]	
$O_2^- + O_3 \rightarrow O_3^- + O_2$	4.0×10^{-10}	[52]	
$O_2^+ + O_2(g,v) + M \rightarrow O_4^+ + M$	$2.4 \times 10^{-30} \times \left(\frac{T_g}{300}\right)^{-3.2}$	[48]	a, b
$O_3^- + M \rightarrow O_3 + M + e^-$	2.3×10^{-11}	[55]	a
$O_3^- + O \rightarrow O_2 + O_2 + e^-$	1.0×10^{-13}	[54]	
$O_3^- + O \rightarrow O_2^- + O_2$	2.5×10^{-10}	[23]	
$O_3^- + O \rightarrow O_3 + O^-$	1.0×10^{-13}	[52]	
$O_3^- + O_3 \rightarrow O_2 + O_2 + O_2 + e^-$	3.0×10^{-10}	[54]	

$O_4^- + O \rightarrow O^- + O_2 + O_2$	3.0×10^{-10}	48	
$O_4^- + O \rightarrow O_3^- + O_2$	4.0×10^{-10}	48	
$O_4^- + O_2 \rightarrow O_2^- + O_2 + O_2$	$1.0 \times 10^{-10} \times \exp\left(-\frac{1044}{T_g}\right)$	29	
$O_4^+ + O \rightarrow O_2^+ + O_3$	3.0×10^{-10}	48	
$O_4^+ + O_2 \rightarrow O_2^+ + O_2 + O_2$	$3.3 \times 10^{-6} \times \left(\frac{300}{T_g}\right)^{4.0} \times \exp\left(-\frac{5030}{T_g}\right)$	48	
$O^- + O_2(a^1\Delta) \rightarrow O_3 + e^-$	3.0×10^{-10}	29	
$O_2^- + O_2(a^1\Delta) \rightarrow O_2 + O_2 + e^-$	2.0×10^{-10}	29	
$O_2^- + O_2(b^1\Sigma^+) \rightarrow O_2 + O_2 + e^-$	3.6×10^{-10}	29	
$O_2^+ + O_2(E_x) + M \rightarrow O_4^+ + M$	$2.4 \times 10^{-30} \times \left(\frac{T_g}{300}\right)^{-3.2}$	29	a, c, d
$O_4^+ + O_2(a^1\Delta) \rightarrow O_2^+ + O_2 + O_2$	1.0×10^{-10}	29	
$O_4^- + O_2(E_x) \rightarrow O_2^- + O_2 + O_2$	1.0×10^{-10}	29	c
$O^- + O_2(a^1\Delta) \rightarrow O_2^- + O$	1.0×10^{-10}	29	
$O^- + O_2(E_x) + M \rightarrow O_3^- + M$	$1.1 \times 10^{-30} \times \exp\left(\frac{300}{T_g}\right)$	29	a, c, e
$O_2^- + O_2(E_x) + M \rightarrow O_4^- + M$	$3.5 \times 10^{-31} \times \exp\left(\frac{T_g}{300}\right)^{-1.0}$	48	a, c, f
$N^+ + N + O_2 \rightarrow N_2^+ + O_2$	1.0×10^{-29}	29	
$N^+ + N_2O \rightarrow NO^+ + N_2$	5.5×10^{-10}	29	
$N^+ + NO \rightarrow N_2^+ + O$	3.0×10^{-12}	29	
$N^+ + NO \rightarrow NO^+ + N$	8.0×10^{-10}	29	
$N^+ + NO \rightarrow O^+ + N_2$	1.0×10^{-12}	29	
$N^+ + O + M \rightarrow NO^+ + M$	1.0×10^{-29}	29	a
$N^+ + O \rightarrow N + O^+$	1.0×10^{-12}	29	
$N^+ + O_2 \rightarrow NO^+ + O$	2.5×10^{-10}	29	
$N^+ + O_2 \rightarrow O^+ + NO$	2.8×10^{-11}	29	
$N^+ + O_2 \rightarrow O_2^+ + N$	2.8×10^{-10}	29	

$N^+ + O_3 \rightarrow NO^+ + O_2$	5.0×10^{-10}	29
$N_2^+ + N_2O \rightarrow N_2O^+ + N_2$	5.0×10^{-10}	29
$N_2^+ + N_2O \rightarrow NO^+ + N + N_2$	4.0×10^{-10}	29
$N_2^+ + NO \rightarrow NO^+ + N_2$	3.3×10^{-10}	29
$N_2^+ + O \rightarrow NO^+ + N$	$1.3 \times 10^{-10} \times \left(\frac{300}{T_{ion}}\right)^{0.5}$	29
$N_2^+ + O_2 \rightarrow O_2^+ + N_2$	$6.0 \times 10^{-11} \times \left(\frac{300}{T_{ion}}\right)^{0.5}$	29
$N_2^+ + O_3 \rightarrow O_2^+ + O + N_2$	1.0×10^{-10}	29
$N_2O^- + N \rightarrow NO + N_2 + e^-$	5.0×10^{-10}	28
$N_2O^- + O \rightarrow NO + NO + e^-$	1.5×10^{-10}	28
$N_2O^+ + NO \rightarrow NO^+ + N_2O$	2.9×10^{-10}	29
$N_3^+ + NO \rightarrow N_2O^+ + N_2$	7.0×10^{-11}	29
$N_3^+ + NO \rightarrow NO^+ + N + N_2$	7.0×10^{-11}	29
$N_3^+ + O_2 \rightarrow NO_2^+ + N_2$	4.4×10^{-11}	29
$N_3^+ + O_2 \rightarrow O_2^+ + N + N_2$	2.3×10^{-11}	29
$N_4^+ + NO \rightarrow NO^+ + N_2 + N_2$	4.0×10^{-10}	29
$N_4^+ + O \rightarrow O^+ + N_2 + N_2$	2.5×10^{-10}	29
$N_4^+ + O_2 \rightarrow O_2^+ + N_2 + N_2$	2.5×10^{-10}	29
$NO^- + N_2O \rightarrow NO + N_2O + e^-$	$4.26 \times 10^{-10} \times \exp\left(-\frac{107.2}{T_g}\right)$	57
$NO^- + NO \rightarrow NO + NO + e^-$	$3.28 \times 10^{-10} \times \exp\left(-\frac{105.1}{T_g}\right)$	57
$NO^- + N \rightarrow N_2O + e^-$	5.0×10^{-10}	29
$NO^- + N_2O \rightarrow NO_2^- + N_2$	2.8×10^{-14}	29
$NO^- + NO_2 \rightarrow NO_2^- + NO$	7.4×10^{-10}	29
$NO^- + O \rightarrow NO_2 + e^-$	1.5×10^{-10}	28
$NO^- + O_2 \rightarrow O_2^- + NO$	5.0×10^{-10}	29
$NO_2^- + N \rightarrow NO + NO + e^-$	5.0×10^{-10}	28

$NO_2^- + N_2O_5 \rightarrow NO_3^- + NO_2 + NO_2$	7.0×10^{-10}	29	
$NO_2^- + NO_2 \rightarrow NO_3^- + NO$	4.0×10^{-12}	29	
$NO_2^- + NO_3 \rightarrow NO_3^- + NO_2$	5.0×10^{-10}	29	
$NO_2^- + O_3 \rightarrow NO_3^- + O_2$	1.8×10^{-11}	29	
$NO_2^+ + NO \rightarrow NO^+ + NO_2$	2.9×10^{-10}	29	
$NO_3^- + N \rightarrow NO + NO_2 + e^-$	5.0×10^{-10}	28	
$NO_3^- + NO \rightarrow NO_2^- + NO_2$	3.0×10^{-15}	29	
$NO_3^- + O \rightarrow NO + O_3 + e^-$	1.5×10^{-10}	28	
$O^- + N \rightarrow NO + e^-$	2.6×10^{-10}	29	
$O^- + N_2(g, v) \rightarrow N_2O + e^-$	0.5×10^{-13}	29	b
$O^- + N_2(A^3\Sigma_u^+) \rightarrow O + N_2 + e^-$	2.2×10^{-9}	29	
$O^- + N_2(B^3\Pi_g) \rightarrow O + N_2 + e^-$	1.9×10^{-9}	29	
$O^- + N_2O \rightarrow N_2O^- + O$	2.0×10^{-12}	29	
$O^- + N_2O \rightarrow NO^- + NO$	2.0×10^{-10}	29	
$O^- + NO + M \rightarrow NO_2^- + M$	1.0×10^{-29}	29	a
$O^- + NO \rightarrow NO_2 + e^-$	2.6×10^{-10}	29	
$O^- + NO_2 \rightarrow NO_2^- + O$	1.2×10^{-9}	29	
$O^+ + N + M \rightarrow NO^+ + M$	1.0×10^{-29}	29	a
$O^+ + N \rightarrow N^+ + O$	1.3×10^{-10}	29	
$O^+ + N_2(g, v) + M \rightarrow NO^+ + N + M$	$6.0 \times 10^{-29} \times \left(\frac{300}{T_{ion}}\right)^2$	29	a, b
$O^+ + N_2(g, v) \rightarrow NO^+ + N$	$(1.5 - 2.0 \times 10^{-3} \times T_{ion} + 9.6 \times 10^{-7} \times T_{ion}^2) \times 1.0 \times 10^{-12}$	29	b
$O^+ + N_2O \rightarrow N_2O^+ + O$	2.2×10^{-10}	29	
$O^+ + N_2O \rightarrow NO^+ + NO$	2.3×10^{-10}	29	
$O^+ + N_2O \rightarrow O_2^+ + N_2$	2.0×10^{-11}	29	
$O^+ + NO \rightarrow NO^+ + O$	2.4×10^{-11}	29	

$O^+ + NO \rightarrow O_2^+ + N$	3.0×10^{-12}	29	
$O^+ + NO_2 \rightarrow NO_2^+ + O$	1.6×10^{-9}	29	
$O_2^- + N \rightarrow NO_2 + e^-$	5.0×10^{-10}	29	
$O_2^- + N_2(B^3\Pi_g) \rightarrow O_2 + N_2 + e^-$	2.5×10^{-9}	29	
$O_2^- + N_2(A^3\Sigma_u^+) \rightarrow O_2 + N_2 + e^-$	2.1×10^{-9}	29	
$O_3^- + N_2(B^3\Pi_g) \rightarrow O_3 + N_2 + e^-$	2.5×10^{-9}	28	
$O_3^- + N_2(A^3\Sigma_u^+) \rightarrow O_3 + N_2 + e^-$	2.1×10^{-9}	28	
$NO^- + N_2(B^3\Pi_g) \rightarrow NO + N_2 + e^-$	2.5×10^{-9}	28	
$NO^- + N_2(A^3\Sigma_u^+) \rightarrow NO + N_2 + e^-$	2.1×10^{-9}	28	
$N_2O^- + N_2(B^3\Pi_g) \rightarrow N_2O + N_2 + e^-$	2.5×10^{-9}	28	
$N_2O^- + N_2(A^3\Sigma_u^+) \rightarrow N_2O + N_2 + e^-$	2.1×10^{-9}	28	
$NO_2^- + N_2(B^3\Pi_g) \rightarrow NO_2 + N_2 + e^-$	2.5×10^{-9}	28	
$NO_2^- + N_2(A^3\Sigma_u^+) \rightarrow NO_2 + N_2 + e^-$	2.1×10^{-9}	28	
$NO_3^- + N_2(B^3\Pi_g) \rightarrow NO_3 + N_2 + e^-$	2.5×10^{-9}	28	
$NO_3^- + N_2(A^3\Sigma_u^+) \rightarrow NO_3 + N_2 + e^-$	2.1×10^{-9}	28	
$O_2^- + NO_2 \rightarrow NO_2^- + O_2$	7.0×10^{-10}	29	
$O_2^- + NO_3 \rightarrow NO_3^- + O_2$	5.0×10^{-10}	29	
$O_2^+ + N \rightarrow NO^+ + O$	1.2×10^{-10}	29	
$O_2^+ + N_2(g, v) + N_2 \rightarrow O_2^+N_2 + N_2$	$9.0 \times 10^{-31} \times \left(\frac{300}{T_{ion}}\right)^2$	29	b
$O_2^+ + N_2(g, v) \rightarrow NO^+ + NO$	1.0×10^{-17}	29	b
$O_2^+ + NO \rightarrow NO^+ + O_2$	6.3×10^{-10}	29	

$O_2^+ + NO_2 \rightarrow NO^+ + O_3$	1.0×10^{-11}	[29]	
$O_2^+ + NO_2 \rightarrow NO_2^+ + O_2$	6.6×10^{-10}	[29]	
$O_2^+N_2 + N_2 \rightarrow O_2^+ + N_2 + N_2$	$1.1 \times 10^{-6} \times \left(\frac{300}{T_{ion}}\right)^{5.3} \times \exp\left(-\frac{2360}{T_{ion}}\right)$	[29]	
$O_2^+N_2 + O_2 \rightarrow O_4^+ + N_2$	1.0×10^{-9}	[29]	
$O_3^- + N \rightarrow NO + O_2 + e^-$	5.0×10^{-10}	[28]	
$O_3^- + NO \rightarrow NO_2^- + O_2$	2.6×10^{-12}	[29]	
$O_3^- + NO \rightarrow NO_3^- + O$	1.0×10^{-11}	[29]	
$O_3^- + NO_2 \rightarrow NO_2^- + O_3$	7.0×10^{-11}	[29]	
$O_3^- + NO_2 \rightarrow NO_3^- + O_2$	2.0×10^{-11}	[29]	
$O_3^- + NO_3 \rightarrow NO_3^- + O_3$	5.0×10^{-10}	[29]	
$O_4^- + N_2 \rightarrow O_2^- + O_2 + N_2$	$1 \times 10^{-10} \times \exp\left(-\frac{1044}{T_g}\right)$	[29]	
$O_4^- + NO \rightarrow NO_3^- + O_2$	2.5×10^{-10}	[29]	
$O_4^+ + N_2(g,v) \rightarrow O_2^+N_2 + O_2$	$4.6 \times 10^{-12} \times \left(\frac{T_{ion}}{300}\right)^{2.5} \times \exp\left(-\frac{2650}{T_{ion}}\right)$	[29]	b
$O_4^+ + NO \rightarrow NO^+ + O_2 + O_2$	1.0×10^{-10}	[29]	

[a] M represents any neutral molecule.

[b] For any species indicated with (g,v), g and v stand for its ground and vibrationally excited state, respectively.

[c] $O_2(E_x)$ represents the electronically excited states: $O_2(a^1\Delta)$ and $O_2(b^1\Sigma^+)$.

[d] The rate coefficient is assumed to be equal to that of $O_2^+ + O_2 + M \rightarrow O_4^+ + M$.

[e] The rate coefficient is assumed to be equal to that of $O^- + O_2 + M \rightarrow O_3^- + M$.

[f] The rate coefficient is assumed to be equal to that of $O_2^- + O_2 + M \rightarrow O_4^- + M$.

Table S.5 Ion-ion reactions included in the model, the corresponding rate coefficient expressions and the references. T_g is the gas temperature in K. The rate coefficients are expressed in $cm^3\ s^{-1} or\ cm^6\ s^{-1}$ for binary or ternary reactions, respectively.

Reaction	Rate coefficient	Ref.	Note
$O^- + O^+ + M \rightarrow O_2 + M$	$1.0 \times 10^{-25} \times \left(\frac{300}{T_g}\right)^{2.5}$	55	a
$O^- + O_2^+ + M \rightarrow O_3 + M$	$1.0 \times 10^{-25} \times \left(\frac{300}{T_g}\right)^{2.5}$	55	a
$O_2^- + O^+ + M \rightarrow O_3 + M$	$1.0 \times 10^{-25} \times \left(\frac{300}{T_g}\right)^{2.5}$	55	a
$O_2^- + O_2^+ + M \rightarrow O_2 + O_2 + M$	$1.0 \times 10^{-25} \times \left(\frac{300}{T_g}\right)^{2.5}$	55	a
$O_3^- + O^+ + M \rightarrow O_3 + O + M$	$2.0 \times 10^{-25} \times \left(\frac{300}{T_g}\right)^{2.5}$	28	a
$O_3^- + O_2^+ + M \rightarrow O_3 + O_2 + M$	$2.0 \times 10^{-25} \times \left(\frac{300}{T_g}\right)^{2.5}$	28	a
$O^- + O_2^+ \rightarrow O + O + O$	$2.60 \times 10^{-8} \times \left(\frac{300}{T_g}\right)^{0.44}$	52	a
$O_3^- + O_2^+ \rightarrow O + O + O_3$	$1.0 \times 10^{-7} \times \left(\frac{300}{T_g}\right)^{0.5}$	52	a
$O^- + O^+ \rightarrow O + O$	$4.0 \times 10^{-8} \times \left(\frac{300}{T_g}\right)^{0.43}$	52	
$O^- + O_2^+ \rightarrow O_2 + O$	$2.6 \times 10^{-8} \times \left(\frac{300}{T_g}\right)^{0.44}$	52	
$O_2^- + O^+ \rightarrow O + O_2$	$2.7 \times 10^{-7} \times \left(\frac{300}{T_g}\right)^{0.5}$	52	
$O_2^- + O_2^+ \rightarrow O_2 + O_2$	$2.01 \times 10^{-7} \times \left(\frac{300}{T_g}\right)^{0.5}$	52	
$O_2^- + O_2^+ \rightarrow O_2 + O + O$	$1.01 \times 10^{-13} \times \left(\frac{300}{T_g}\right)^{0.5}$	52	

$O_3^- + O^+ \rightarrow O_3 + O$	$1.0 \times 10^{-7} \times \left(\frac{300}{T_g}\right)^{0.5}$	56	
$O_3^- + O_2^+ \rightarrow O_2 + O_3$	$2.0 \times 10^{-7} \times \left(\frac{300}{T_g}\right)^{0.5}$	52	
$NO^- + A^+ + M \rightarrow NO + A + M$	$2.0 \times 10^{-25} \times \left(\frac{300}{T_g}\right)^{2.5}$	28	a, b
$NO_2^- + A^+ + M \rightarrow NO_2 + A + M$	$2.0 \times 10^{-25} \times \left(\frac{300}{T_g}\right)^{2.5}$	28	a, b
$N_2O^- + A^+ + M \rightarrow N_2O + A + M$	$2.0 \times 10^{-25} \times \left(\frac{300}{T_g}\right)^{2.5}$	28	a, b
$NO_3^- + A^+ + M \rightarrow NO_3 + A + M$	$2.0 \times 10^{-25} \times \left(\frac{300}{T_g}\right)^{2.5}$	28	a, b
$O_3^- + B^+ + M \rightarrow O_3 + B + M$	$2.0 \times 10^{-25} \times \left(\frac{300}{T_g}\right)^{2.5}$	28	a, c

[a] M represents any neutral molecule.
[b] A represents N, O, N_2, O_2, NO, NO_2 and N_2O species.
[c] B represents N, N_2, NO, NO_2 and N_2O species.

Table S.6 Optical transitions of N_2 and O_2 molecules. The Einstein transition probabilities are expressed in s^{-1}.

Reaction	Rate coefficient	Ref.	Note
$N_2(A^3\Sigma_u^+) \rightarrow N_2$	0.5	29	
$N_2(B^3\Pi_g) \rightarrow N_2(A^3\Sigma_u^+)$	1.35×10^5	29	
$N_2(a'^1\Sigma_u^-) \rightarrow N_2$	1.0×10^2	29	
$N_2(C^3\Pi_u) \rightarrow N_2(B^3\Pi_g)$	2.45×10^7	29	
$O_2(a^1\Delta) \rightarrow O_2$	2.6×10^{-4}	29	
$O_2(b^1\Sigma^+) \rightarrow O_2$	8.5×10^{-2}	29	

$O_2(b^1\Sigma^+) \rightarrow O_2(a^1\Delta)$	1.5×10^{-3}	[29]	
$O_2(A^3\Sigma^+, C^3\Delta, c^1\Sigma^-) \rightarrow O_2$	11	[29]	a

[a] $O_2(A^3\Sigma^+, C^3\Delta, c^1\Sigma^-)$ is a combination of three electronic excited states at a threshold energy of 4.5 eV.

The reaction rate coefficient expressions of the V-T relaxations and V-V exchanges between N_2-N_2, O_2-O_2, N_2-O_2 are calculated using the Forced Harmonic Oscillator (FHO) model proposed by Adamovich et al.[58] This method offers a semi-classical non-perturbative analytical solution for V-T and V-V transitions of diatomic molecules by averaging the V-T and V-V probabilities (P_{VT} and P_{VV}) over the one-dimensional Boltzmann distribution.

$$P_{VT}(i \rightarrow f) = \frac{(n_s)^s}{(s!)^2} \cdot \varepsilon^s \cdot \exp\left(-\frac{2n_s}{s+1}\varepsilon\right) \quad (10)$$

$$P_{VV}(i_1, i_2 \rightarrow f_1, f_2) \cong \frac{\left[n_s^{(1)} n_s^{(2)}\right]^s}{(s!)^2} \cdot \left(\frac{\rho_\varepsilon^2}{4}\right)^s \cdot \exp\left[-\frac{2n_s^{(1)} n_s^{(2)}}{s+1}\frac{\rho_\varepsilon^2}{4}\right] \quad (11)$$

with $s = |i - f|$, $n_s = \left[\frac{\max(i,f)!}{\min(i,f)!}\right]^{1/s}$. $\rho_\varepsilon$and ε are collision and potential specific parameters.

Table S.7 Vibrational-vibrational exchanges and vibrational-translational relaxations for N_2 (as an example) and the rate coefficient expressions.

Reaction	**Rate coefficient**
$N_2(v_i) + M \rightarrow N_2(v_i - 1) + M$	$Z \cdot \left(\frac{m}{kT}\right) \int_0^\infty P_{VT}(\bar{v}) \cdot \exp\left(\frac{-mv^2}{2kT}\right)$ vdv
$N_2(v_i) + N_2(v_j) \rightarrow N_2(v_i - 1) + N_2(v_j + 1)$	$Z \cdot \left(\frac{m}{kT}\right) \int_0^\infty P_{VV}(\bar{v}) \cdot \exp\left(\frac{-mv^2}{2kT}\right)$ vdv

M represents any neutral molecule in the plasma.

v_i and v_j are the vibrational levels of N_2 (0-24).

Z is the collision frequency and v is the particle velocity.

The reaction rates coefficients of the V-T relaxations between N_2-N are based on quasi-classical calculations that have been reproduced through a fit as proposed by Esposito et al.[59], for the following general reaction:

$N_2(v) + N \rightarrow N_2(w) + N$, with $v > w$

All the relevant trends in the reaction rate coefficient were taken into consideration by using an additive model into the exponential argument of the reaction rate constant, as shown in the following expression (valid for $v = 1 - 66$ and $\Delta v = 1 - 30$):

$$k(v, T, \Delta v) = \exp\left(a_1(v, \Delta v) + \frac{a_2(v, \Delta v)}{T} + \frac{a_3(v, \Delta v)}{T^2} + \frac{a_4(v, \Delta v)}{T^3} + a_5(v, \Delta v) \cdot \ln(T)\right) \quad (12)$$

where

$$a_i(v, \Delta v) = z_{i0}(\Delta v) + z_{i1}(\Delta v)v + z_{i2}(\Delta v)v^2 + z_{i3}(\Delta v)v^3 + z_{i4}(\Delta v)v^4 \quad (13)$$

$$z_{ij}(\Delta v) = b_{ij} + c_{ij}\Delta v \quad (14)$$

for which the parameters are reported in [59].

Similarly, the reaction rate coefficients of the V-T relaxations between O_2-O are based on quasi-classical calculations that have been reproduced through a fit as proposed by Esposito et al.[60], for the following general reaction:

$O_2(v) + O \rightarrow O_2(w) + O$, with $v > w$

The reaction rate constant is then determined based on the following expression:

$$k(T, v, \Delta v) = DegF \cdot \exp\left(a_1(v, \Delta v) + \frac{a_2(v, \Delta v)}{\ln(T)} + a_3(v, \Delta v) \cdot \ln(T)\right) \quad (15)$$

where Δv is $(v - w)$

$$a_i(v, \Delta v) = b_{i1}(\Delta v) + b_{i2}(\Delta v) \cdot \ln(v) + \frac{b_{i3}(\Delta v) + b_{i4}(\Delta v)v + b_{i5}(\Delta v)v^2}{10^{21} + \exp(v)} \quad (15)$$

$$b_{ij}(\Delta v) = c_{ij1} + c_{ij2} \cdot \ln(\Delta v) + c_{ij3} \cdot \Delta v \cdot \exp(-\Delta v) + c_{ij4} \cdot \Delta v \cdot \Delta v \quad (16)$$

The coefficients c_{ijk} have been generated using a linear least squares method and are reported in [60] where the degenary factor (DegF) is also explained.

REFERENCES

1 Y. Gorbanev, E. Vervloessem, A. Nikiforov and A. Bogaerts, *ACS Sustain. Chem. Eng.*, 2020, **8**, 2996–3004.
2 A. V. Pipa and R. Brandenburg, *atoms*, 2019, **7**, 2–18.
3 S. Liu and M. Neiger, *J. Phys. D. Appl. Phys.*, 2003, **36**, 3144–3150.
4 K. H. R. Rouwenhorst, F. Jardali, A. Bogaerts and L. Lefferts, *Energy Environ. Sci.*, 2021, **14**, 2520–2534.
5 B. Zhao, L. He, H. Du and H. Zhang, *Plasma Sci. Technol.*, 2014, **16**, 370–373.
6 Q. Xiong, A. Y. Nikiforov, X. P. Lu and C. Leys, *J. Phys. D. Appl. Phys.*, 2010, **43**, 415201.
7 I. Korolov, D. Steuer, L. Bischoff, G. Hübner, Y. Liu, V. Schulz-Von der Gathen, M. Böke, T. Mussenbrock and J. Schulze, *J. Phys. D. Appl. Phys.*, , DOI:10.1088/1361-6463/abd20e.
8 P. J. Bruggeman, N. Sadeghi, D. C. Schram and V. Linss, *Plasma Sources Sci. Technol.*, , DOI:10.1088/0963-0252/23/2/023001.
9 G. J. M. Hagelaar and L. C. Pitchford, *Plasma Sources Sci. Technol.*, 2005, **14**, 722–733.
10 M. A. Lieberman and A. J. Lichtenberg, *Principles of Plasma Discharges and Materials Processing: Second Edition*, Wiley-Interscience, 2nd Editio., 2005.
11 Y. Gorbanev, E. Vervloessem, A. Nikiforov and A. Bogaerts, *ACS Sustain. Chem. Eng.*, 2020, **8**, 2996–3004.
12 www.comsol.com, *COMSOL Multiphysics v. 5.4*.
13 E. Vervloessem, M. Aghaei, F. Jardali, N. Hafezkhiabani and A. Bogaerts, *ACS Sustain. Chem. Eng.*, 2020, **8**, 9711–9720.
14 V. Laporta, D. A. Little, R. Celiberto and J. Tennyson, *Plasma Sources Sci. Technol.*, 2014, **23**, 065002.
15 L. L. Alves, *J. phys. Conf. Ser.*
16 Morgan database, www.lxcat.net, retrieved in february 2018.
17 Itikawa database, www.lxcat.net, retrieved in february 2018.
18 V. Laporta, R. Celliberto and J. Tennyson, *plasma sources sci. Technol.*, 2013, **22**, 025001.
19 Y. Itikawa, *J. Phys. Chem. Ref. Data*, 2009, **38**, 1–20.
20 Y. Itikawa, *J. Phys. Chem. Ref. Data*, 2009, **38**, 1–20.
21 B. Eliasson and U. Kogelschatz, *Basic Data for Modelling of Electrical Discharges in Gases: Oxygen*, Baden: ABB Asea Brown Boveri, 1986.
22 S. A. Lawton and A. V. Phelps, *J. chem. Phys.*, 1978, **69**, 1055–1068.
23 L. E. Khvorostovskaya and V. A. Yankovsky, *Contrib. to Plasma Phys.*, 1991, **31**, 71–88.
24 H. Hokazono, M. Obara, K. Midorikawa and H. Tashiro, *J. Appl. Phys.*, 1991, **69**, 6850–6868.
25 Quantemol database, www.lxcat.net, retrieved in february 2018.
26 Hayashi database, www.lxcat.net, retrieved in february 2018.
27 F. J. Gordillo-V'azquez, *J. Phys. D. Appl. Phys.*, 2008, **41**, 234016–234049.
28 W. Wang, R. Snoeckx, X. Zhang, M. S. Cha and A. Bogaerts, *J. Phys. Chem. C*, 2018, **122**, 8704–8723.
29 Capitelli, *Plasma Kinetics in Atmospheric Gases*, Springer, 2000.
30 D. J. Kewley and H. G. Hornung, *Chem. Phys. Lett.*, 1974, **25**, 531–536.
31 M. A. A. Clyne and D. H. Stedman, *J. Phys. Chem.*, 1967, **71**, 3071–3073.
32 W. Van Gaens and A. Bogaerts, *J. Phys. D. Appl. Phys.*, 2014, **47**, 079502 (3pp).
33 W. Tsang and R. F. Hampson, *J. Phys. Chem. Ref. Data*, 1986, **15**, 1087–1279.
34 R. Atkinson, D. L. Baulch, R. A. Cox, R. F. Hampson, J. A. Kerr Chairman and J. Troe, *J. Phys. Chem. Ref. Data*, 1997, **18**, 881–1097.
35 H. Hippler, R. Rahn and J. Troe, *J. Chem. Phys.*, 1990, **93**, 6560–6569.

36 J. M. Heimerl and T. P. Coffee, *Combust. Flame*, 1979, **35**, 117–123.
37 G. Suzzi Valli, R. Orrú, E. Clementi, A. Laganà and S. Crocchianti, *J. Chem. Phys.*, 1995, **102**, 2825–2832.
38 D. L. Baulch, C. J. Cobos, R. A. Cox, P. Frank, G. Hayman, T. Just, J. A. Kerr, T. Murrells, M. J. Pilling, J. Troe, R. W. Walker and J. Warnatz, *J. Phys. Chem. Ref. Data*, 1994, **23**, 847–1033.
39 J. Hjorth, J. Notholt and G. Restelli, *Int. J. Chem. Kinet.*, 1992, **24**, 51–65.
40 J. T. Herron, *J. Chem. Phys.*, 1961, **35**, 1138–1139.
41 P. P. Bemand, M. A. A. Clyne and R. T. Watson, *J. Chem. Soc. Faraday Trans. 2 Mol. Chem. Phys.*, 1974, **70**, 564–576.
42 R. Atkinson, D. L. Baulch, R. A. Cox, J. N. Crowley, R. F. Hampson, R. G. Hynes, M. E. Jenkin, M. J. Rossi, J. Troe, P. R. Center, L. H. Science, T. Centre and S. Park, *J. Phys. Chem. Ref. Data*, 2004, **I**, 1461–1738.
43 W. Tsang and J. T. Herron, *J. Phys. Chem. Ref. Data*, 1991, **20**, 609–663.
44 R. A. Graham and H. S. Johnston, *J. Phys. Chem.*, 1978, **82**, 254–268.
45 P. G. Ashmore and M. G. Burnett, *J. Chem. Soc. Faraday Trans. 2*, 1962, 253–261.
46 I. M. Campbell and B. A. Thrush, *Trans. Faraday Soc.*, 1966, **62**, 3366–3374.
47 W. L. Nighan, *Phys. Rev.*, 1970, **2**, 1989–2000.
48 I. A. Kossyi, A. Y. Kostinsky, A. A. Matveyev and V. P. Silakov, *Plasma Sources Sci. Technol.*, 1992, **1**, 207–220.
49 R. E. Beverly, *Opt. Quantum Electron.*, 1982, **14**, 501–513.
50 S. Pancheshnyi, B. Eismann, G. J. M. Hagelaar and L. C. Pitchford, Computer code ZDPlaskin, http://www.zdplaskin.laplace.univ-tlse.fr.
51 M. Whitaker, M. A. Biondi and R. Johnsen, *Phys. Rev. A*, 1981, **24**, 743–745.
52 J. T. Gudmundsson and E. G. Thorsteinsson, *Plasma Sources Sci. Technol.*, 2007, **16**, 399–412.
53 A. A. Ionin, I. V. Kochetov, A. P. Napartovich and N. N. Yuryshev, *J. Phys. D. Appl. Phys.*, 2007, **40**, R25–R36.
54 A. Cenian, A. Chernukho and V. Borodin, *Contrib. to Plasma Phys.*, 1995, **35**, 273–296.
55 T. G. Beuthe and J.-S. Chang, *Jpn. J. Appl. Phys.*, 1997, **36**, 4997–5002.
56 B. Eliasson, M. Hirth and U. Kogelschatz, *J. Phys. D. Appl. Phys.*, 1987, **20**, 1421–1437.
57 M. Mcfarland, D. B. Dunkin, F. C. Fehsenfeld, A. L. Schmeltekopf and E. E. Ferguson, *J. Chem. Phys.*, 1972, **56**, 2358–2364.
58 I. V. Adamovich, S. O. MacHeret, J. W. Rich and C. E. Treanor, *J. Thermophys. Heat Transf.*, 2008, **12**, 57–65.
59 F. Esposito, I. Armenise and M. Capitelli, *Chem. Phys.*, 2006, **331**, 1–8.
60 F. Esposito, I. Armenise, G. Capitta and M. Capitelli, *Chem. Phys.*, 2008, **351**, 91–98.